

Gas pile-up, gap overflow, and Type 1.5 migration in circumbinary disks: application to supermassive black hole binaries

Bence Kocsis^{1,3*}, Zoltán Haiman^{2†} and Abraham Loeb^{1‡}

¹*Harvard-Smithsonian Center for Astrophysics, 60 Garden St., Cambridge, MA 02138, USA*

²*Department of Astronomy, Columbia University, 550 West 120th Street, New York, NY 10027*

³*Einstein Fellow*

3 November 2018

ABSTRACT

We study the interaction of a supermassive black hole (SMBH) binary and a standard radiatively efficient thin accretion disk. We examine steady-state configurations of the disk and migrating SMBH system, self-consistently accounting for tidal and viscous torques and heating, radiative diffusion limited cooling, gas and radiation pressure, and the decay of the binary’s orbit. We obtain a “phase diagram” of the system as a function of binary parameters, showing regimes in which both the disk structure and migration have a different character. Although massive binaries can create a central gap in the disk at large radii, the tidal barrier of the secondary causes a significant pile-up of gas outside of its orbit, which can lead to the closing of the gap. We find that this spillover occurs at an orbital separation as large as $\sim 200M_7^{-1/2}$ gravitational radii, where $M_\bullet = 10^7 M_7 M_\odot$ is the total binary mass. If the secondary is less massive than $\sim 10^6 M_\odot$, then the gap is closed before gravitational waves (GWs) start dominating the orbital decay. In this regime, the disk is still strongly perturbed, but the piled-up gas continuously overflows as in a porous dam, and crosses inside the secondary’s orbit. The corresponding migration rate, which we label Type 1.5, is slower than the usual limiting cases known as Type I and II migration. Compared to an unperturbed disk, the steady-state disk in the overflowing regime is up to several hundred times brighter in the optical bands. Surveys such as PanSTARRS or LSST may discover the periodic variability of this population of binaries. Our results imply that the circumbinary disks around SMBHs can extend to small radii during the last stages of their merger, when they are detectable by *LISA*, and may produce coincident electromagnetic (EM) emission similar to active galactic nuclei (AGN).

Key words: accretion, accretion discs – black hole physics – gravitational waves – galaxies: active

1 INTRODUCTION

1.1 Overview

Understanding the coevolution of binaries and the accretion disks in which they are embedded is critical in several fields of astrophysics, including planet formation and migration (Goldreich & Tremaine 1980; Ward 1997), patterns in planetary rings (Goldreich & Tremaine 1982), stellar binaries (Shu et al. 1987; McKee & Ostriker 2007), the final parsec phase of black hole binaries (Begelman et al.

1980; Escala et al. 2005; Lodato et al. 2009), stars and black holes (BHs) in active galactic nuclei (Goodman & Tan 2004; Miralda-Escudé & Kollmeier 2005; Levin 2007), and electromagnetic (EM) counterparts to gravitational wave (GW) events (Kocsis et al. 2008; Haiman et al. 2009; Schnittman 2011). These systems may also provide observational probes to test models of the anomalous viscosity in accretion disks (Kocsis et al. 2011; Yunes et al. 2011).

Despite the long history of the subject, there are very few self-consistent analytic models for the coevolution of binaries and accretion disks, incorporating the fundamental physical effects over the long timescales on which the binary separation evolves. The standard α -model of radiatively efficient turbulent thin accretion disks (Shakura & Sunyaev

* E-mail: bkocsis@cfa.harvard.edu

† E-mail: zoltan@astro.columbia.edu

‡ E-mail: aloeb@cfa.harvard.edu

1973) relates the effective kinematic viscosity of the disk to the pressure $\nu \propto \alpha p$. The viscous evolution of the disk, however, is often modeled without considering the pressure dependence of the viscosity (Lynden-Bell & Pringle 1974). Similarly, models of the gravitational interaction between the disk, which describe the launching of spiral density waves in the disk that remove angular momentum from the binary, also do not account for the tidal heating of the disk and the corresponding feedback on the torques (Goldreich & Tremaine 1980).

In an accompanying paper (Kocsis et al. 2012, hereafter Paper I) we derive an analytic steady-state model for the coevolution of the disk and the orbital migration of the secondary, in which we combine a Shakura & Sunyaev (1973) disk with the theory of the binary-disk interaction by Goldreich & Tremaine (1980) self-consistently. In particular, we adopt the viscosity prescription for standard thin α or β disks, calculate the sound speed and vertical balance including both gas and radiation pressure (p_{gas} and p_{rad}), adopt a simple analytic approximation to the angular momentum exchange between the binary and the disk of Armitage & Natarajan (2002), consider the viscous and tidal heating of the disk (Lodato et al. 2009), and self-consistently account for the feedback on the pressure, viscosity, scaleheight, and the torque cutoff near the secondary's orbit, as well as on the migration rate of the secondary. We derive azimuthally averaged analytic disk models which recover the Goodman & Tan (2004) solution for arbitrary $\beta = p_{\text{gas}}/(p_{\text{gas}} + p_{\text{rad}})$ in the limit that the secondary mass m_s approaches zero. The solution is then generalized for larger m_s , i.e. to the case when the disk structure is significantly modified by the secondary, over multiple accretion timescales.

In this paper, we explore the implications of the new binary+disk evolution solutions, found in Paper I, for SMBH binary systems. By varying the binary parameters systematically, we explore possible distinct behaviors of the disk-secondary system. We recover the two limiting cases known previously, and identify a new intermediate phase. Low-mass objects perturb the disk only weakly, and the linear density perturbations lead to the extensively studied *Type-I migration* of the secondary (Goldreich & Tremaine 1980). For very massive objects, the tidal torque clears a gap in the disk, and the viscous radial inflow of the gas pushes the object inward (known as *Type-II migration*). A particular subclass of the latter is the so-called secondary-dominated Type-II migration, in which the secondary's mass exceeds the nearby gas mass, causing the migration to slow down, and the surface density outside of the gap to build up, before it is able to efficiently push the object inward (Syer & Clarke 1995). This assumes that the pile-up is 100% efficient and no gas can cross the secondary's orbit. We identify a separate, intermediate class of migration, *Type-1.5*, in which the gas piles up significantly outside of the perturber's orbit, but the viscosity increases to the point that in steady-state, the gas enters the nonlinear gravitational field of the secondary (i.e. its Hill sphere), and is able to flow across its orbit. Not surprisingly, the corresponding migration rate is significantly different from both the Type I and II cases.¹

¹ The non-axisymmetric part of the perturbations may be

In most previous investigations, the gap opening conditions were based on the comparison of viscous and tidal torques in a weakly perturbed disk (Crida et al. 2006; Armitage 2007; Kocsis et al. 2011). The orbital decay of the binary and the evolution of the disk density profile is then coupled; this coupled evolution has not been followed on the long time-scales on which the orbit evolves. Although a cavity may indeed be opened at large radii, in accretion disks where the gas build-up outside the cavity is significant, the cavity may close after several accretion timescales. Our solutions allow us to derive the long-term gap opening and closing criteria.

There are many possible observational implications of our findings for black hole binaries, and perhaps also for planetary dynamics. Here we restrict our attention to the former context. First, gap-closing makes it more likely that GW inspiral events are accompanied by EM emission, since the binary is embedded in a gaseous disk, with no central cavity, even at the last stages of the merger. Previously, Liu et al. (2003) and Milosavljević & Phinney (2005) have argued that as the GW inspiral accelerates beyond the rate at which the gas at the edge of the cavity can viscously follow the binary, the binary decouples from the disk. Consequently, they argued that luminous AGN (active galactic nuclei) or radio emission from jets are expected only after the gas has had time to accrete onto the remnant. The post-merger delay is between years and decades for binaries in the mass range 10^5 – $10^6 M_\odot$ expected to be detectable by *eLISA/NGO*² (Amaro-Seoane et al. 2012; see also Tanaka et al. 2010; Tanaka & Menou 2010; Shapiro 2010). However, if the central cavity refills before the GW emission becomes significant (which we find is the case in the above mass range, in particular), then the gas can accrete onto the primary and shine much like a normal bright AGN, even during the last stages of the merger, producing coincident EM counterparts or precursors to *LISA* sources.

Second, gas accumulation outside of the secondary leads to a greatly enhanced surface brightness (Lodato et al. 2009). This may help in searches for EM counterparts to more massive (10^8 – $10^9 M_\odot$) SMBH binaries at larger separations, still in the gas-driven stage, emitting GWs in the pulsar timing array frequency bands (Tanaka et al. 2012; Sesana et al. 2012). The EM spectrum of the disk missing the emission at high frequencies if the disk has a gap (Syer & Clarke 1995), and the bright gap edge has a characteristic ultraviolet-optical-infrared profile (Lodato et al. 2009). We investigate the brightening as a function of component masses and separations. If these sources produce correspondingly bright periodic EM variability on the orbital timescale, they can be identified in future time-domain optical/IR surveys. The statistics of many such sources can observationally test the migration and GW inspiral rates (Haiman et al. 2009). Combining the predictions for the variability timescale, disk brightness, and spectrum offers

either linear or non-linear depending on the magnitude of pile-up. In both cases, we adopt the tidal torque model of Armitage & Natarajan (2002), reminiscent of Type-I migration, which we use with the azimuthally-averaged self-consistent disk profile (see Paper I).

² <http://elisa-ngo.org/>

new independent tests of the physical models of the accretion physics, disk-satellite interactions, and GW emission.

Goodman & Tan (2004) and McKernan et al. (2012) pointed out that supermassive stars or intermediate mass black holes (IMBHs) in the range 10^2 – $10^5 M_\odot$ may form in AGN disks. These objects would perturb the accretion disk, causing a pile up and gap overflow as described here. Our studies imply a slow-down of migration for these objects, making these systems longer-lived, and thus increasing the likelihood of their detection.

1.2 Relation to previous works

Without the aim of completeness, we highlight here the similarities and main differences between our study and some related papers in the recent literature.

Based on the solutions of Zel’dovich & Raizer (1967) and Pringle (1991), Ivanov et al. (1999) showed that the circumbinary disk with a binary evolves in a self-similar way on scales much larger than the binary, assuming that the initial and outer boundary conditions represent an unperturbed stationary α -disk with a fixed \dot{M} , and assuming that a gap is always present which truncates the disk within the secondary and causes the radial gas velocity to be effectively zero near the secondary (see also Rafikov 2012). Here, we examine the opposite limiting case in which the radial gas velocity is nonnegligible near the secondary due to gap overflow and the disk is approximately in a steady-state.

Chang et al. (2010) examined the coevolution of the disk and the secondary, and found that the former may exhibit a rapid brightening in the GW driven regime as the binary shepherds gas inward before merger (however, see Baruteau et al. 2012). They included almost the same physics as this study and solved the time dependent equations in 1 dimension numerically for a binary with 10^7 and $10^6 M_\odot$ mass components. Their initial conditions were that of an unperturbed disk and focussed on the final GW driven regime. In this case, they found no gas overflow across the gap.

Liu & Shapiro (2010) constructed an analytic steady-state model, and showed that the disk may brighten significantly when an object is placed in the disk (locally by a factor of 10^4 for a mass ratio $q = 0.1$). However, they have considered a constant H/r (here H is the disk scaleheight and r is the radius) and a viscosity profile corresponding to an unperturbed disk, and neglected the changes in these quantities due to the secondary.

Lodato et al. (2009) considered a disk model whose local physics is very similar to ours, but solved the time evolution numerically in 1 dimension for a very different choice of initial and boundary conditions. In particular, they focused on the specific case where the SMBH binary is very massive, and has a “one-time” disk that is much less massive, compact (spreading over at most a factor of 10 in radii) and is not replenished by accreting new material from large radii. They found gas pileup outside the secondary, leading to a brightening of the outer disk, and a modified spectrum. Their numerical results provide a useful independent reference to qualitatively verify our steady-state radial disk surface density and scaleheight profiles. For the particular binaries they have considered, the migration rate was greatly reduced, such that the binary is not transported to the

GW-driven regime within a Hubble time, and they showed that this poses an obstacle against solving the final parsec problem (Begelman et al. 1980). In our paper, we examine the steady-state configuration, under the assumption of a constant accretion rate in the disk (set by the Eddington limit near the primary). This assumes a constant mass supply from larger radii, and is therefore very different from the “one-time” disk in Lodato et al. (2009). As a result, we reach essentially the opposite conclusions: we find a stronger pileup, which increases radiation pressure in the disk and stabilizes it against gravitational fragmentation, and yields a much faster migration (well within the Hubble time). Another practical difference in our study is that we consider a broad range of binary masses, mass ratios and semimajor axes, including the radiation pressure dominated regime, and we map out the distinct phases for disk structure and migration.

Most studies on planetary migration neglect the tidal heating effect and radiation pressure, and are therefore inapplicable for our purposes. We investigate AGN accretion disks where radiation effects are more significant. Interestingly, we find that the disk becomes strongly radiation pressure dominated outside the secondary, even in regions far from the primary, which, in the absence of the secondary, would be gas pressure dominated. Therefore, this requires treating the fluid as comprised of both gas and radiation. The use of a single equation of state parameter, as in most papers in planetary dynamics, becomes invalid in this regime. We note that D’Angelo et al. (2003) did account for tidal heating and temperature variations in a two-dimensional simulation, but neglected the effects of radiation pressure. Paardekooper & Mellema (2006, 2008) and Kley & Crida (2008) presented results from numerical simulations with radiation, showing that tidal heating and radiation pressure have a significant effect on the migration of planets.

Criteria for gap opening and closing have been investigated extensively for protoplanetary disks (Lin & Papaloizou 1986; Artymowicz & Lubow 1994; Ward 1997; Crida et al. 2006). Previous numerical studies typically neglected the effects of gas build-up outside the gap, and did not consider self-consistently the effects of the excess viscous and tidal heating of the gas, and neglected both radiation pressure and the migration of the secondary. However, two- and three-dimensional simulations have shown that even if the gap opening conditions are satisfied, gas can periodically flow in along non-axisymmetric streams into the gap and accrete onto the primary and the planet, particularly if the ratio of the distance to the gap edge to the Hill radius is of order unity (Artymowicz & Lubow 1996; Lubow et al. 1999; Lubow & D’Angelo 2006; Hayasaki et al. 2007; MacFadyen & Milosavljević 2008; Cuadra et al. 2009). In this paper, we revisit the standard gap opening/closing conditions in circumbinary accretion disks, including the effects of radiation pressure (Kocsis et al. 2011), as well as gas build-up, tidal heating, and migration. For simplicity, we neglect a possible non-axisymmetric inflow if the gap is larger than the Roche lobe and also neglect accretion onto the secondary. We also do not model the magneto-rotational instability (MRI), which may influence the conditions for gap opening (Winters et al. 2003; Noble et al. 2012;

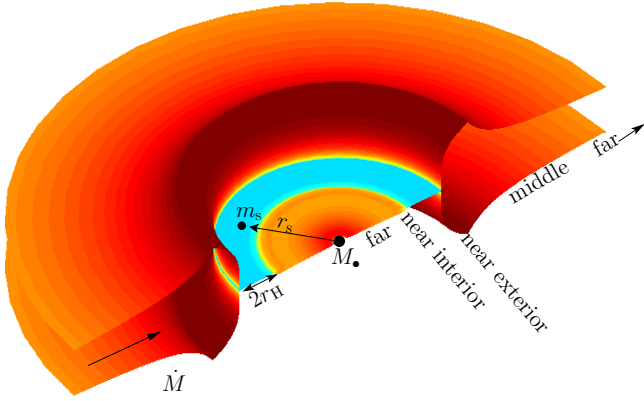


Figure 1. Gas pile-up and overflow in a circumbinary accretion disk with component masses M_\bullet and m_s , binary separation r_s , and accretion rate \dot{M} . We distinguish five distinct radial zones in the disk: an inner and an outer far zone where the effects of the secondary are negligible, an interior and an exterior near zone, where the tidal effects are significant, and an extended middle zone, where the disk is still significantly perturbed. Our model breaks down inside the secondary’s Hill radius, denoted by r_H .

Shi et al. 2012; Farris et al. 2012). These effects are likely to be important, and should be investigated in the future in two- or three-dimensional simulations.

1.3 Outline and conventions

This paper is organized as follows. In § 2, we briefly lay out the physical model that we adopt. In § 3, we present numerical and analytic solutions to the disk and identify its distinct physical phases. In § 4, we elaborate on the gap opening and closing conditions in steady-state. In § 5, we discuss the migration of the secondary, comparing the new Type-1.5 solution in a continuously overflowing disk with the Type-I and Type-II cases. In § 6, we discuss observable implications, including the lightcurve, spectrum, the abundance of AGN with periodic variability, as well as GW observations with *LISA/NGO* and pulsar timing arrays (PTAs, Hobbs et al. 2010). We summarize our main conclusions in § 7. The interested reader can find details of analytic derivations in Paper I.

Our basic notation for the disk and secondary parameters are depicted in Figure 1. We denote the primary and secondary mass with M_\bullet and m_s , and the mass ratio with $q \equiv m_s/M_\bullet$. We use geometrical units $G = c = 1$ and suppress factors of G/c^2 and G/c^3 in conversions between mass, length, and time units. We use $\bar{r} \equiv r/(GM_\bullet/c^2)$ to label the radius in gravitational radii. A subscript “s” refers to quantities describing the secondary, while the subscript “0” refers to quantities in the unperturbed disk around a single compact object.

2 THERMO-HYDRODYNAMICAL INTERACTION BETWEEN A DISK AND A SECONDARY

We examine the evolution of the secondary and an azimuthally and vertically averaged Shakura-Sunyaev disk (i.e. axisymmetric one-zone disk) in local thermal equilibrium.

The equations are laid out in detail, and solved both numerically and under various approximations, analytically in Paper I. Here we only briefly summarize the basic conceptual framework and the features of the solutions; we refer the reader to Paper I for the complete set of equations and a detailed description.

2.1 Equations governing the evolution of the disk structure and the binary’s orbit

We denote the azimuthally-averaged surface density profile of the disk by $\Sigma(r)$, and the radial (bulk) velocity of the gas in the disk by $v_r(r) = -\dot{M}/[2\pi r\Sigma(r)]$, which is negative as gas accretes toward the primary at $r = 0$ with an accretion rate \dot{M} . We assume a nearly Keplerian disk and denote the angular velocity with Ω .

Assuming that the migration velocity of the secondary, v_{sr} is sufficiently slow, the disk evolves through a sequence of steady-state configurations, where $\dot{M}(r) = \dot{M}$ is a constant. The angular momentum flow in the disk is driven by the viscous torques (T_ν) and the tidal torque exerted by the secondary (T_d), while the angular momentum loss of the secondary is due to the backreaction of the tidal torque and gravitational wave losses

$$\dot{M}\partial_r(r^2\Omega) = \partial_r T_\nu - \partial_r T_d, \quad (1)$$

$$\dot{L}_s = \frac{1}{2}m_s r_s \Omega_s v_{sr} = -\int_0^\infty \partial_r T_d dr - T_{\text{GW}}, \quad (2)$$

Here

$$T_\nu = -2\pi r^3(\partial_r\Omega)\nu\Sigma \simeq 3\pi r^2\Omega\nu\Sigma, \quad (3)$$

$$\partial_r T_d = 2\pi r\Lambda\Sigma, \quad (4)$$

$$T_{\text{GW}} = \frac{32}{5}\frac{m_s^2}{M_\bullet}\bar{r}_s^{-7/2}, \quad (5)$$

where we adopt the widely-used approximation of Armitage & Natarajan (2002) for the specific tidal torque,

$$\Lambda \approx \begin{cases} -\frac{1}{2}fq^2r^2\Omega^2r^4/\Delta^4 & \text{if } r < r_s - r_H, \\ +\frac{1}{2}fq^2r^2\Omega^2r^4/\Delta^4 & \text{if } r > r_s + r_H, \end{cases} \quad (6)$$

where

$$\Delta \equiv \max(|r - r_s|, H). \quad (7)$$

Equation (6) breaks down in the region near the secondary’s orbit, i.e. within its Hill radius or tidal radius, $|r - r_s| < r_H \equiv (q/3)^{1/3}r_s$. We excise this region from our calculations and instead match the interior and exterior solutions, setting $T_\nu(r_s - r_H) = T_\nu(r_s + r_H)$. This has an effect similar to smoothing the torques inside the Hill radius, as done previously in Lin & Papaloizou (1986), Syer & Clarke (1995), and Lodato et al. (2009). Here, $q \equiv m_s/M_\bullet$, $H \ll r$ is the scaleheight of the disk, and f is a constant calibrated with simulations. We conservatively adopt the low value $f_{-2} \equiv f/10^{-2} = 1$ for our numerical solutions, but the dependence on f_{-2} is explicitly computed in the analytic solutions.

Given the viscosity $\nu(r)$ and the scale-height $H(r)$, Eq. (1) can be integrated to find the surface density of the disk, $\Sigma(r)$, for any location of the secondary, and Eq. (2) gives the inward migration velocity of the secondary (Liu & Shapiro 2010). However $\nu(r)$ and $H(r)$ are not known a priori, since they depend on $\Sigma(r)$ and the

mid-plane temperature $T_c(r)$, with the standard Shakura-Sunyaev ansatz $\nu(r) = \alpha c_s(r)H(r)$ for viscosity or its variant where the viscosity is assumed to scale with the gas (rather than the total) pressure, $\nu(r) = \alpha c_s(r)H(r)\beta(r)$, where $\beta(r) \equiv p_{\text{gas}}(r)/p(r)$ (also known as a “ β -disk”). Since α disks are thought to suffer from a thermal instability (but see Hirose et al. 2009), in the solutions discussed in this paper, we follow earlier work and focus on the latter case (also known as a “ β -disk”). We derive the temperature profile assuming thermal equilibrium between gas and radiation, radiative cooling which balances the heating associated with viscous dissipation tidal heating. These provide a non-linear closed set of equations for the steady-state disk profile. In practice, we note that all of the equations are nonlinear local algebraic equations at each radius with the exception of the angular momentum flux equation (1) which is a first-order ordinary differential equation for $T_\nu(r)$. We solve these equations for specific boundary conditions given below, for a fixed value of the secondary orbital radius. Once the disk profile has been obtained, Eq. (2) gives the migration velocity of the secondary.

2.2 Boundary conditions

We look for steady-state disk solutions with a constant \dot{M} , assuming that the radial profile of the disk relaxes on a time-scale shorter than the migration time-scale of the secondary. We find the corresponding equilibrium steady-state configuration of the disk for each orbital radius of the secondary, and then assume that the disk proceeds through a sequence of such steady-state configurations as the secondary migrates inwards.

We distinguish two types of inner boundary conditions, corresponding to whether or not a gap is assumed to be present in the steady-state configuration.

I. Boundary condition without a cavity. We here assume that the gas can continuously overflow, crossing the secondary’s orbit, and the surface density is finite ($\Sigma(r) \neq 0$) throughout the disk all the way to the primary’s innermost stable circular orbit r_{ISCO} . We then adopt the zero-torque inner boundary condition usually assumed in accretion disks onto a single point mass (Novikov & Thorne 1973; Penna et al. 2010; Tanaka 2011; Zhu et al. 2012), i.e. we require

$$T_\nu(r_{\text{ISCO}}) = 0. \quad (8)$$

Starting with this boundary condition, we obtain all properties of the disk, including the gas velocity profile $v_r(r)$, as well as the radial speed of the secondary v_{sr} . If the disk is strongly perturbed³, the solution is self-consistent if $|v_r(r)| \gg |v_{\text{sr}}|$ over a wide range of radii around the secondary, so that the disk can relax sufficiently rapidly to steady-state. In practice, we assume approximate steady-state if $v_r(\lambda r_s) \geq \lambda v_{\text{sr}}$ (where the constant $\lambda \gtrsim 1$ will be introduced below). Otherwise, the secondary outpaces the nearby gas inflow, and if the disk is strongly perturbed, we assume a gap opens. We discuss gap opening in detail in § 4.

³ i.e. the viscous torque is greatly reduced (increased) in the near zone interior (exterior) to the secondary’s orbit relative to the solitary disk without a secondary

II. Boundary condition for a truncated disk. If the tidal torques dominate over the viscous torques near the secondary, gas is expelled from the region near the secondary and we assume that a circular cavity forms in the disk. In the cases we consider, the secondary mass is sufficiently large that the gas piles up significantly outside the cavity. The tidal torque acting on the inner edge of the disk has a sharp cutoff (Eq. 6). We define a characteristic radius in the disk outside the gap, where the tidal torque is exerted on the disk⁴ $r_g = \lambda r_s$ and assume that the density enhancement at this radius tracks the inward migration of the secondary in a self-similar way, preserving a constant ratio of radii $\lambda = r_g/r_s$. This requires that the gas velocity at r_g satisfies

$$v_r(r_g) = \frac{r_g}{r_s} v_{\text{sr}}. \quad (9)$$

Note that λ is not specified by hand ab-initio; it is found self-consistently in our solutions (see below and in Paper I). This condition can be understood intuitively, since the secondary cannot “run away” and leave the outer disk behind (if it did, it would cease to be able to torque the disk and would have to slow down). Likewise, the gap edge cannot be moving closer to the secondary (at least not on time-scales faster than the migration timescale; if it did, then the gap would close and the steady-state solution would be inconsistent). Although with a moving gap, the disk cannot strictly be in steady-state near its boundary, we assume $\dot{M}(r) \approx \dot{M}$ at $r > r_g$ (see discussion below).

By construction, only one of the above two boundary conditions will lead to a self-consistent solution. We speculate that a real time-dependent binary would evolve through the sequence of steady-state solutions we obtain below – switching between the case with and without a gap around the transition radii that follows from the above.

We emphasize that the solutions with a gap are somewhat similar to those obtained in previous works (Syer & Clarke 1995), and also that our solutions in this regime still suffer from a few possible inconsistencies, as will be discussed below. However, the main new result in this paper is the independent overflowing solution, corresponding to the first of the two boundary conditions. As we will argue below, the assumptions leading to this regime are relatively more robust. The uncertainties about the behavior of the disk with a gap could affect only our results for when the gap closes (as argued below, we took a conservative approach, in the sense that the “overflow” regime may be present for a wider range of radii than in our fiducial models).

3 DISK STRUCTURE

3.1 Numerical solutions

In Figure 2, we present the most relevant physical parameters in our steady-state disk as a function of radius (we neglected T_{GW} for clarity in this figure) for several choices of parameters. For details on how these solutions were obtained in practice, the reader is again referred to Paper I. As the figure shows, the secondary acts as a hydro dam and

⁴ In our numerical solutions we define r_g as the radius where the tidal torque density drops to 10% of its peak value, although our results are insensitive to this precise choice.

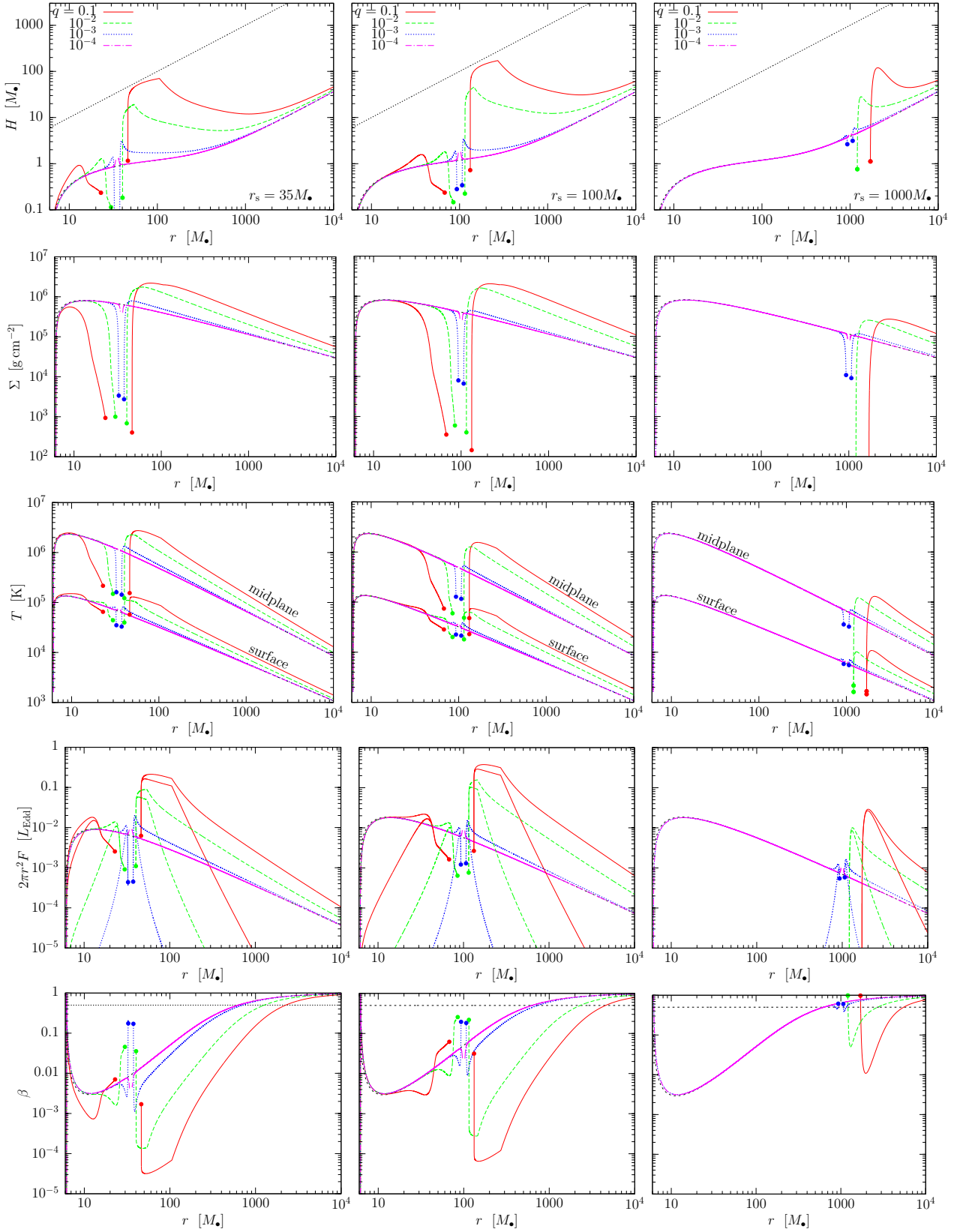


Figure 2. Steady-state tidally heated disks with the secondary located at $r_s = \{35, 100, 1000\} M_\bullet$ (left, center, right panels) for various mass ratios $q = m_s/M_\bullet = 10^{-n}$ with $n \in \{1, 2, 3, 4\}$ (red, green, blue, magenta curves) for $M_\bullet = 10^7 M_\odot$. The five different rows from top to bottom show the local scaleheight, surface density, surface and midplane temperature, surface brightness and tidal heating, and the gas to total pressure ratio. The magenta curve with $q = 10^{-4}$ is similar to a solitary disk without a secondary. An inner cavity forms in the disk for $q = 0.1$ and 0.01 for $r = 1000 M_\bullet$ on the right panels. The gas continuously overflows for the other cases shown in the figure, but the surface density can still drop significantly near the secondary’s Hill sphere (marked by filled circles). (For clarity, the curves are not connected within the Hill sphere, where our model becomes invalid.)

causes gas to pile-up (second row) and heat up (third row) relative to the unperturbed solution. Interestingly, the disk brightens not only in the near zone of the secondary, where the tidal effects dominate, but even much farther away (see the panels in the 4th row showing the disk brightness relative to the tidal heating rate). This is not surprising, since viscosity needs to balance the tidal torque at the boundary in equilibrium, and pushing the gas past this obstacle requires a greatly accumulated local gas-mass, even far from this region. Our results are in qualitative agreement with the radial profiles presented in Lodato et al. (2009).

Of the 12 cases shown in Figure 2 with $r_s = (35, 100, 1000)M_\bullet$ and $q = (10^{-1}, 10^{-2}, 10^{-3}, 10^{-4})$, a gap forms only in the two cases with the largest binary separations and mass ratios: $r_s = 1000M_\bullet$ with $q = 0.1$ and 0.01 (red and green curves on the right panels). In these cases, there is no inner disk interior the secondary's orbit in the steady-state configuration (if there was it would accrete onto the SMBH without being replenished from the outside). All other cases *do not* have a gap.⁵ To avoid confusion, we note that the profiles are not shown within the Hill sphere of the secondary in Fig. 2. Although our working assumptions break down, the parameters are expected to transition continuously across this region.

One may identify visually distinct zones in the radial profiles of the physical parameters in Fig. 2. At very large radii, which we call the *far zone*, the disk asymptotes to the unperturbed state. Interior to a certain radius, in the *exterior middle zone*, the scaleheight starts to deviate initially gradually then quite rapidly as the radiation pressure becomes significant relative to the gas pressure. Note that the transition to a radiation pressure dominated disk (i.e. $\beta < 0.5$) is around $600M_\bullet$ without a secondary. However, the disk can become radiation pressure dominated outside a secondary much farther out as shown by the 5th row (c.f. dotted black line showing $\beta = 0.5$). In the *near zone* of the satellite, the tidal effects become significant. For relatively massive binaries, the sharp knee in the tidal heating rate, as seen in the 4th row, corresponds to the torque cutoff where the midplane pressure gradient shifts the tidal effects out of resonance ($H \sim |r - r_s|$).⁶ After crossing the radius of the secondary's orbit, the accretion velocity is more rapid than for an unperturbed disk by many orders of magnitude (see Figure 5 below). The disk profile asymptotes to the unperturbed disk profile near the inner boundary close to the SMBH. Note however, that the tangential velocity ($v_t \sim (r/M_\bullet)^{-1/2}c$) and sound speed ($c_s \sim (H/r)v_t$) are much larger than the radial velocity even in this region.

We will discuss migration rates in detail in § 5 below, but let us mention already which of the 12 cases shown in Figure 2 correspond to the well-known Type-I and II cases. The two cases $r_s = 1000M_\bullet$ with $q = 0.1$ or 0.01 have a gap, and thus imply Type-II migration. The case with $q = 10^{-4}$ and $r_s = 35M_\bullet$ corresponds to Type-I migration,

where the disk structure lies close to the unperturbed case. The 7 cases with $q \geq 10^{-3}$ without a gap have a significantly perturbed overflowing disk, which corresponds to the distinct new class of Type 1.5 migration. The remaining two cases with $q = 10^{-4}$ and with $r_s = (100, 1000)M_\bullet$ are between Type I and 1.5. However, comparing the disk-driven migration speed with the GW inspiral rate, we find that GW emission is significant for many of these binaries, so that the steady-state assumption is violated (see Fig. 4 below for the conditions under which this occurs).

3.2 Analytic solutions

To generalize the numerical solutions given above for arbitrary parameters, we derived in Paper I approximate analytic formulas. These solutions exist in different regions where either the tidal, the viscous torques, or the angular momentum flux is negligible relative to the other two terms in Eq. (1). In particular, we identify the two *far zones*, well outside and far inside the secondary's orbit, where the effects of the secondary are negligible, a single *middle zone* outside the secondary's orbit, where the disk structure is greatly modified but where the tidal torque and heating are negligible, and two *near zones* just inside and outside r_s , where the tidal effects dominate. We distinguish two possible cases for the middle zone, depending on whether the disk has a gap or if the disk is overflowing. In the external near zone, we likewise have two possible behaviors, depending on whether the tidal torque is unsaturated or saturated (i.e. whether the torque cutoff is in play: $\Delta = |r - r_s|$ or H in Eq. (6), respectively). We refer the reader to Paper I for detailed derivations of the analytic solution for the disk structure in each zone; here we provide only the most important results, and discuss their implications for SMBH binaries.

The physical parameters at radius r in the disk are given by

$$X(r, r_s, \mathbf{p}) = C \alpha_{-1}^{c_1} \dot{m}_{-1}^{c_2} M_7^{c_3} r_2^{c_4} f_{-2}^{c_5} q_{-3}^{c_6} r_{s2}^{c_7} \Phi(r, r_s, \mathbf{p}) \quad (10)$$

where X denotes any of $\{\Sigma, T_c, H, v_r, F, T_\nu\}$; r_2 and r_{s2} denote the radial distance from the primary and the orbital radius of the secondary in units $100M_\bullet$, respectively; and $\Phi(r, r_s, \mathbf{p})$ denotes an extra function of the parameters which is different in different zones. The constant parameters C and c_i and Φ are given explicitly in Paper I (see Table 1 therein). Here we only discuss the structure of the solution.

The steady-state viscous torque density T_ν in different regions constitutes the backbone of the analytic solution. Every physical quantity in the disk follows directly from T_ν by simple arithmetic relations. To verify the analytic model with the numerical solutions of § 3.1, it is sufficient to examine T_ν in the various regions. We do this by generating the numerical solution for randomly chosen constant model parameters ($\alpha, \dot{m}, f, M_\bullet, q, r_s$), and compare these to the analytic solution. We find a good agreement between the two solutions to within 20% for a wide range of parameters for which T_ν is substantially modified exterior to the r_s . We do not develop analytic approximations in the opposite, weakly perturbed case, because in that regime other physical processes which have been neglected may be more significant (see Type-I migration in § 5.1).

The analytic solution is self-consistent in the strongly

⁵ Here by “gap” we mean regions in which $\Sigma(r) = 0$ (i.e. $r < r_0$ where $r_0 > r_s + r_H$ falls outside the Hill radius; see above). Regardless, note that $\Sigma(r)$ can be greatly decreased in the overflowing solutions near the secondary.

⁶ Note that the changes seem deceptively abrupt on a logarithmic scale. To see this, consider $y = (x - 1)^2$, a smooth function, that exhibits a similar feature on a log-log plot near $x = 1$.

perturbed case if T_ν matches continuously in the different zones outside the Hill sphere. In practice, note that T_ν increases in the external near zone quite rapidly with radius, both in the tidal torque-saturated and unsaturated regimes. At larger radii, the tidal effects vanish (middle zone) and T_ν is approximately constant. If T_ν in the middle zone without a gap is lower than with a gap, then this represents the correct overflowing solution; otherwise a gap forms. Since for a steady-state disk, the migration rate is simply proportional to T_ν in the middle zone (see Eq. 30 in Paper I), this definition is equivalent to that based on the velocities (Eq. 9). If so, the secondary and the gas propagate inward with similar velocities to maintain this configuration, while in the former case, the secondary moves slower than the inflow speed of the gas. We elaborate on these issues related to gap opening and migration in § 4 and 5 below.

We emphasize that the disk parameters can differ dramatically from the unperturbed (or far zone) values not only in the near zone, where the tidal effects dominate, but also in the middle zone, where tidal effects are already negligible. This is analogous to how the water level is raised in a dam not just in the immediate vicinity of the dam wall but even far away from the boundary, regions in which the local hydrodynamics is explicitly independent of the wall. The tidal effects of the secondary are also short-range, but the corresponding effect is communicated to distant regions by setting an effective boundary condition. The middle region subtends a large radial range, and is representative of the strongly perturbed disk. Here, the viscous torque T_ν^m (in all three cases: with a gap, or overflowing with saturated or unsaturated torques; see the corresponding solutions T_ν^{mg} , T_ν^{mos} , and T_ν^{mou} in Table 1 of Paper I) is approximately constant with radius as in a *decretion disk* (Pringle 1991). It is remarkable that the perturbation to the disk can be represented by a single number in the middle zone. Here, the radial profile of the disk is independent of the details of the tidal torque up to this constant factor.

Rather than using T_ν^m , we introduce a more physically revealing quantity, $k \equiv T_\nu^m/T_{\nu 0}$, representing the fractional change of the viscous torque relative to its unperturbed value ($T_{\nu 0} = \dot{M}r^2\Omega$) in the middle zone. This parameter, which we refer to as the dimensionless angular momentum flux or *brightening factor*, sets the relative brightening of the disk and the increase in the scaleheight in the middle zone, as well as the migration rate. It can take one of three values, depending on whether a gap is open, or whether the gas overflows in the saturated torque cutoff regime or in the

unsaturated regime⁷:

$$k_s^{\text{mg}} = 23 \alpha_{-1}^{1/2} \dot{m}_{0.1}^{-3/8} M_7^{-3/4} q_{-3}^{5/8} \lambda^{-11/16} r_{s2}^{-7/8} \quad (11)$$

$$k_s^{\text{mos}} = 0.97 \alpha_{-1}^{-2/11} \dot{m}_{-1}^{-1} M_7^{1/22} f_{-2}^{5/22} q_{-3}^{5/11} r_{s2}^{39/44} \times [-\mathcal{W}(-a)]^{13/11}, \quad (12)$$

$$k_s^{\text{mou}} = 1.3 \alpha_{-1}^{-2} \dot{m}_{-1}^{-1} M_7^{1/2} f_{-2}^{5/2} q_{-3}^{5/2} r_{s2}^{-1/4} \times \left[1 + \left(\frac{\delta r_i}{r_s} \right)^{1/3} \right]^{-115/24} \left(\frac{\delta r_i}{r_H} \right)^{-15/2}. \quad (13)$$

Here $\mathcal{W}(-a)$ is the Lambert W-function defined for $a > 1/e = 0.368$ approximately as

$$|\mathcal{W}(-a)| \approx -\ln(-a) + \ln(-\ln(a)) \quad (14)$$

where

$$a = 0.465 \alpha_{-1} f_{-2}^{-5/4} q_{-3}^{-13/12} M_7^{-1/4} r_{s2}^{5/8} \left(\frac{\delta r_i}{r_H} \right)^{17/4}. \quad (15)$$

In practice, $1 \lesssim |\mathcal{W}(-a)| \lesssim 10$ for a wide range of parameters. In the above equations, δr_i is the radial distance from r_s at which the torque model breaks down near the secondary, for which we assume $\delta r_i \sim r_H$. Further, λr_s is the characteristic radius in the near zone outside the gap where most of the tidal torque is exerted. In practice, λ is of order unity given by Eq. (41) below.

The smallest of the three, $k_s = \min(k_s^{\text{mg}}, k_s^{\text{mos}}, k_s^{\text{mou}})$, sets the state of the disk in the middle zone if greater than one.⁸ Note that k_s^{mg} increases quickly with decreasing binary separation, r_s , but interior to some radius the gap closes and the dimensionless angular momentum flux or brightening factor is limited by the near-zone torque cutoff, k_s^{mos} . The brightening factor is largest at the gap-closing boundary for comparable mass ratios. The torque cutoff does not impose a limitation if q is sufficiently small, but the gap can still close by shrinking to within the Hill radius (in this case k_s^{mou} sets the brightening factor).

Figure 3 shows the phase diagram of the disk for different r_s and q , set by Eqs. (11–13) for $M_\bullet = 10^5, 10^7$, and $10^9 M_\odot$. Colors indicate the brightening factor, k_s . The figure shows large deviations from a solitary disk in many cases. The disk brightens in the middle zone by a factor of up to 500 or 100 for a binary with $M_\bullet = 10^5$ or $10^7 M_\odot$, respectively, which we discuss in § 6. The brightening is less significant for binaries with $10^9 M_\odot$. Note that GW emission is neglected here; this modifies the picture at small radii significantly, especially for $M_\bullet = 10^9 M_\odot$ (see Fig. 4 below).

We note that these solutions assume a steady-state. However, in Paper I we have shown that the steady-state assumption is strongly violated by the inward migration of the secondary in the case of a truncated disk with a central cavity if \dot{M} is fixed at the outer boundary (Syer & Clarke

⁷ The brightening factor has a simple radial dependence in the middle zone $k \propto r^{-1/2}$. We extrapolate the brightening factor in the middle zone to the location of the secondary, typically a conservative estimate of the true brightening of the disk outside the secondary's orbit as this neglects the excess brightening due to tidal heating in the near zone (see Paper I).

⁸ We do not consider the cases where either k_s^{mg} , k_s^{mos} , or k_s^{mou} is less than one. In this case, the analytic solutions need further modifications (see Paper I).

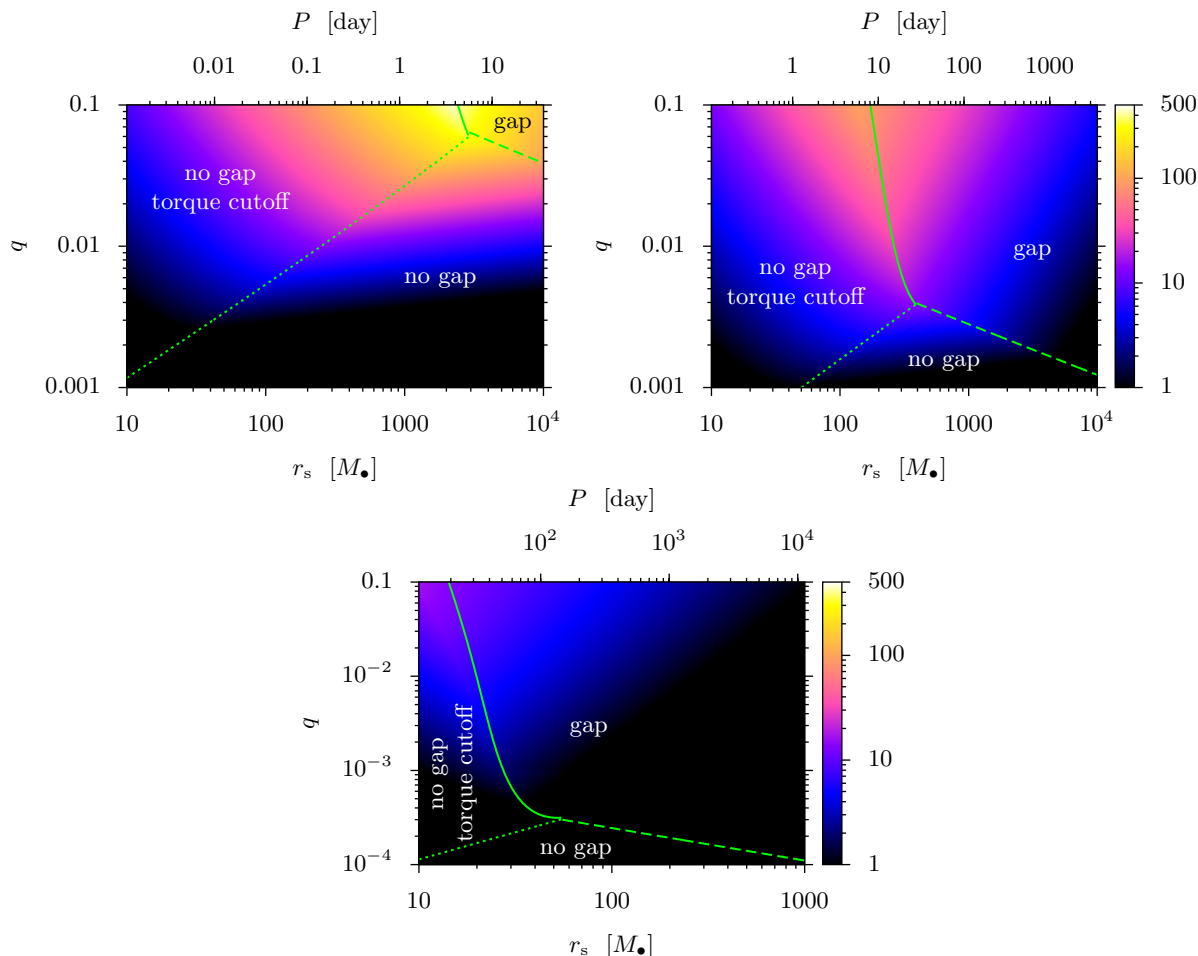


Figure 3. The phase diagram of the disk for $M_* = 10^5 M_\odot$ (top left) $10^7 M_\odot$ (top right) and $10^9 M_\odot$ (bottom) and for different binary semimajor axes, orbital periods, and mass ratios. Colors show the relative brightening of the disk outside the secondary relative to the same region of a solitary disk. Three zones can be distinguished as marked: “gap” in which the tidal torque can support a gap against viscosity even in steady-state, “no gap” in which the gap overflows in steady-state with the tidal torque in the linear regime all the way to the Hill sphere or “no gap with torque cutoff” in which the torques are saturated outside the Hill sphere. We do not show comparable mass ratios ($q > 0.1$) where the adopted perturbative tidal torque formula and the axisymmetric steady-state approximations are strongly violated.

1995, see however discussion in § 5.2). In contrast, steady-state is possible in the overflowing case because there k_s decreases as the secondary moves inwards. A global steady-state is possible if $k_s \lesssim k_{\max}$ where

$$k_{s \max} = 3.2 |\gamma_{\Sigma_s}|^{5/19} \alpha_{-1}^{4/19} \dot{m}_{-1}^{-3/19} M_7^{6/19} q_{-3}^{5/19} r_{s2}^{-7/19}. \quad (16)$$

A similar requirement for a global steady-state in a radiation pressure dominated α -disk is less restrictive. For larger k_s , an approximate steady-state with a fixed \dot{M} may still hold locally in the inner regions of the middle zone, but in this case, the outer parts of the middle zone within $r \sim k_s^2 r_s$ cannot respond to the inward migration of the secondary and the steady-state disk model becomes inaccurate there (see further discussion in § 5.2).

We finally comment on the stability of the accretion disk in the middle zone. Although the surface density increases as gas accumulates outside the secondary as $k^{3/5}$, the radiation pressure grows even more rapidly as $p_{\text{rad}} \propto k$ in that region (see Eqs. 40–41 in Paper I). The net effect is to increase the Toomre- Q parameter as $Q \propto c_s/\Sigma \propto$

$p_{\text{rad}}/\Sigma \propto k^{2/5}$. Therefore, the enhanced radiation pressure dominates over the increase in surface density, and makes the disk more stable against axisymmetric fragmentation relative to an unperturbed disk without a secondary (Tanaka et al. 2012). Although gravitationally stable, the disk may become dynamically unstable against global non-axisymmetric perturbations if the disk develops a steep pressure gradient in the near zone around a high-mass secondary (Papaloizou & Pringle 1985; Goldreich et al. 1986). A proper stability analysis, and exploring its implications, is left to future work.

4 GAP OPENING

Next we elaborate on the gap opening and closing conditions in more detail. Gap opening is traditionally examined by comparing the tidal and viscous torques in an initially unperturbed steady-state thin disk. However, after a sufficient amount of gas has built up outside the gap, the enhanced

viscous torque may close the gap. We discuss these points in turn.

Gap opening also affects the migration rate of the secondary and has several potentially observable signatures which we discuss in § 5 and 6.

4.1 Initial gap-opening

The velocity of the gas and the secondary can be computed starting from Eqs. (1) and (2) [see Paper I for details]:

$$v_r = -\frac{\partial_r T_\nu}{2\pi r \Sigma \partial_r (r^2 \Omega)} + \frac{\Lambda}{\partial_r (r^2 \Omega)} = -\frac{\dot{M}}{2\pi r \Sigma}, \quad (17)$$

$$v_{sr} = -\frac{2}{m_s \Omega_s r_s} \left(\int_0^\infty \partial_r T_d dr + T_{GW} \right). \quad (18)$$

where negative values represent an inward motion.

Consider a secondary placed in an initially unperturbed disk, and examine the conditions for the local gas flow to be reversed. This is equivalent to finding the region $v_r(r_0) \geq 0$ in Eq. (17), which is where the tidal torques dominate over the viscous torques, or where the tidal timescale is smaller than the viscous timescale in an unperturbed disk. Substituting T_ν from Eq. (3) and Λ from Eq. (6), and assuming that $r = r_s + \Delta$ where $\Delta \ll r_s$, setting $v_r = 0$ in Eq. (17), we find

$$\frac{\Delta_0}{r_s} = \left(\frac{f}{3k_{\nu 0}} \frac{q^2 r_s^2 \Omega_s}{\nu_0} \right)^{1/3}, \quad (19)$$

where ν_0 is the unperturbed viscosity near the secondary, and $k_{\nu 0} = d \ln T_{\nu 0} / d \ln \Delta = 1/2$ is the radial exponent of the unperturbed viscous torque near r_s . Comparing Eq. (19) with gas pressure dominated locally isothermal hydrodynamical numerical simulations with no tidal heating, gives a prefactor in the range $3k_{\nu 0}/f \sim 40\text{--}50$ (Crida et al. 2006), which implies $f = 0.03\text{--}0.04$.

Two conditions are required⁹ for the tidal torques to initially truncate the disk and create a gap after inserting an object into the disk (Syer & Clarke 1995; Ward 1997; Crida et al. 2006):

$$\Delta_0 \gtrsim H_0 \quad \text{and} \quad \Delta_0 \gtrsim r_H. \quad (20)$$

First, the maximum tidal torque, which corresponds to a distance $\Delta_0 \sim H_0$, needs to exceed the viscous torque to keep gas from flowing in. Inside this distance, the tidal torque saturates due to the ‘‘torque cutoff’’ and cannot counteract the viscous torque (Goldreich & Tremaine 1980) (see also discussion below Eq. [6]). Thus, gap opening requires, $\Delta_0 \gtrsim H_0$. Second, the derivation of the torque formula assumed that the effect of the secondary is a small perturbation to the gravitational potential; this assumption breaks down interior to the Hill sphere. Thus, consistency also requires $\Delta_0 \gtrsim r_H$. Gas may be expected to accrete onto the secondary or to cross the gap, if this condition is violated. In addition to violating the conditions in Eq. (20), a gap may also close by 3D overflow if $H \gtrsim r_s$. However, Ward (Ward

⁹ The gap opening conditions are sometimes written as $\Delta_0 \gtrsim r_H \gtrsim H_0$, where $r_H \gtrsim H_0$ is the condition for the azimuthal perturbations to become nonlinear (Ward 1997; Korycansky & Papaloizou 1996). We shall not require $r_H \gtrsim H_0$ here over the two conditions in Eq. (20).

1986, 1988) has shown that using the 2D midplane torque gives a result typically within 20% to the vertically averaged torque (see however Jang-Condell & Sasselov 2005), so that the gap closes by midplane inflow in typical cases, and additional criteria are not necessary.

These gap opening criteria translate into bounds on the mass ratio for fixed r_s (Lin & Papaloizou 1986; Crida et al. 2006) where

$$q \gtrsim q_{s0} = \sqrt{\frac{3k_{\nu 0}}{f} \frac{\nu_0}{r_s^2 \Omega_s}} \left(\frac{H_0}{r_s} \right)^{3/2}, \quad \text{and} \quad (21)$$

$$q \gtrsim q_{u0} = \frac{k_{\nu 0}}{f} \frac{\nu_0}{r_s^2 \Omega_s}, \quad (22)$$

If $q \lesssim q_{s0}$ the gap is closed by viscosity as the tidal torque saturates due to the pressure gradients, and if $q \lesssim q_{u0}$ it is closed by the near-field gravity of the secondary. Thus, after releasing an object in a radiation pressure dominated α or β disk, a gap opens if (Kocsis et al. 2011)

$$q_{\alpha 0} \gtrsim \max \left\{ 4.5 \times 10^{-5} \frac{\alpha_{-1}^{1/2} \dot{m}_{-1}^{5/2}}{f_{-2}^{1/2} r_{s2}^{5/2}}, 5.7 \times 10^{-4} \frac{\alpha_{-1} \dot{m}_{-1}^2}{f_{-2} r_{s2}^2} \right\} \quad (23)$$

$$q_{\beta 0} \gtrsim \max \left\{ 2.0 \times 10^{-5} \alpha_{-1}^{2/5} \dot{m}_{-1}^{17/10} M_7^{-1/10} f_{-2}^{-1/2} r_{s2}^{-29/20}, 4.0 \times 10^{-5} \alpha_{-1}^{4/5} \dot{m}_{-1}^{2/5} M_7^{-1/5} f_{-2}^{-1} r_{s2}^2 \right\} \quad (24)$$

while for gas pressure dominated accretion disks

$$q_{\text{gas}0} \gtrsim \max \left\{ 1.7 \times 10^{-6} \alpha_{-1}^{1/4} \dot{m}_{-1}^{1/2} M_7^{-1/4} f_{-2}^{-1/2} r_{s2}^{1/8}, 4.0 \times 10^{-5} \alpha_{-1}^{4/5} \dot{m}_{-1}^{2/5} M_7^{-1/5} f_{-2}^{-1} r_{s2}^{1/10} \right\}. \quad (25)$$

Here, the first and second terms in each parentheses correspond to q_{s0} (Eq. 21) and q_{u0} (Eq. 22), respectively. Note that latter is the same for gas and radiation pressure dominated regimes for a β disk because this condition, Eq. (22), is independent of H , and because ν is insensitive to radiation pressure in the β model.

Figure 4 shows the gap opening criteria for β disks with our standard parameters as a function of mass ratio and binary separation for $M_\bullet = 10^{5,7,9} M_\odot$. The blue solid and the dashed curves represent q_{s0} and q_{u0} , respectively. For smaller mass ratios, the disk is practically unperturbed.

4.2 Steady-state gap-closing

In the regime where a gap never opens (i.e. weakly perturbed disks, $q < q_{\text{crit}0}$), our solutions do not change the picture. However, in the regime when a gap initially opens, the accumulation of gas outside the binary changes Σ , H , ν , and k_ν in the gap-opening conditions, Eqs. (19–20). Let us now examine whether the gap can stay open on longer timescales once the disk and binary have reached steady-state.

As the binary migrates inwards the local pressure and viscosity change even in an unperturbed disk, which may lead to gap opening for mass ratios of order $q \sim 10^{-4}$ within separations $r_s \sim 10^3 M_\bullet$ (see blue lines in Figure 4). However, the usual gap opening conditions Eqs. (21–22) (Lin & Papaloizou 1986; Syer & Clarke 1995) may fail in the long run and lead to gap-closing for a much wider range of masses and radii, if either the scaleheight, the viscosity, or the steepness of the radial profile increases during the

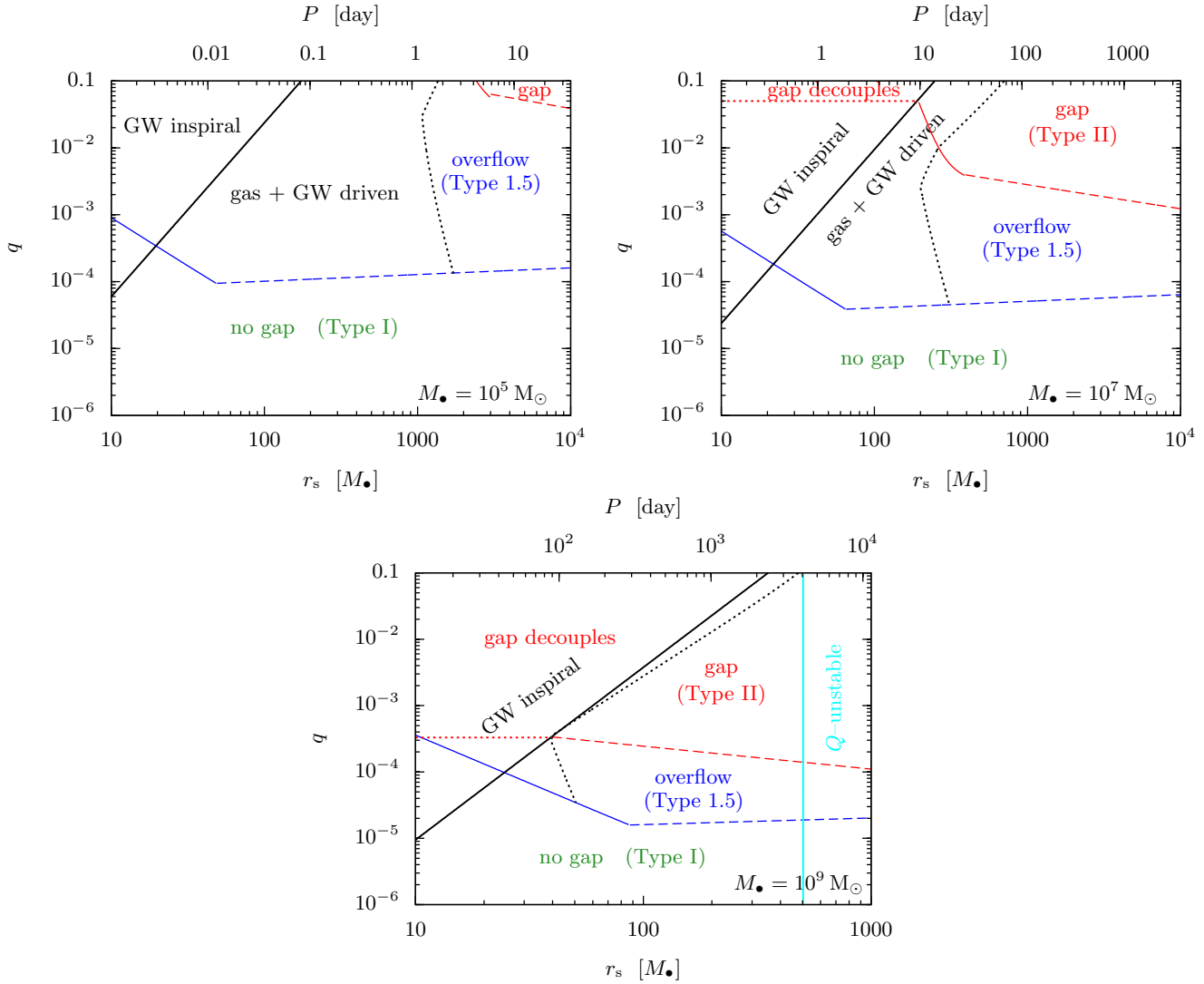


Figure 4. Ranges of binary separation r_s and mass ratio q for which: (i) a gap can remain open in the disk; (ii) the gap refills after gas pileup (labeled as “overflow”), and (iii) a gap cannot open. Different panels show different primary masses (10^5 , 10^7 , and $10^9 M_\odot$) as labeled. The type of migration is shown in each region, including the region where GW losses start to become relevant (dotted line) and where they dominate (solid black line). Solid and dashed colored lines show the boundary where the tidal torque becomes saturated outside the Hill sphere (viscous filling, $\Delta = H$) and where the gas enters the Hill sphere without becoming saturated (gravitational filling, $\Delta = r_H$), respectively, based on standard criteria using unperturbed disks. The gap (if present) decouples in the GW inspiral regime as shown. The disk is gravitationally unstable at large radii as marked.

pile-up. Note that if only H increased by a factor x while ν and k_ν were kept constant, then the mass ratio for gap opening would increase by $x^{3/2}$ relative to the first terms in Eqs. (23–25). Furthermore, if ν or k_ν changed by a factor y , then the the critical mass ratio for gap opening would further increase by an extra factor of \sqrt{y} and y in the first and second terms in Eqs. (23–25), respectively. Thus, the combination of these effects shifts the solid and dashed blue lines in Figure 4 upwards by a factor $x^{3/2}y^{1/2}$ and y , respectively. We determine the actual value of x and y in the self-consistent steady-state model to derive the necessary conditions for gap opening next.

In a self-consistent decription, gas accumulation outside the gap leads to the following effects. First, the gravitational torque of a denser disk drives the migration of the secondary faster, increasing $|v_{sr}|$ (see Eqs. 4 and 18). For a fixed ac-

cretion rate, $\dot{M} = 2\pi r|v_r|\Sigma$, the increase of Σ leads to the decrease of $|v_r|$, analogous to the slowdown of the flow velocity in a river upstream a dam. The pressure and kinematic viscosity increases due to the pile-up, and leads to a smaller gap. The tidal heating in the gas outside the disk increases the pressure and scaleheight further which can quench the tidal torque (see torque cutoff in Eq. 6). Ultimately, the combination of these effects can have several outcomes.

(i) If the mass of the secondary is very small, the disk is weakly perturbed (no gap is present in particular) and the object exhibits Type-I migration as usual (see § 5).

(ii) The other extreme limit is Type-II migration, where $|v_{sr}| = |v_r(\lambda r_s)|/\lambda$ is reached so that the disk and the secondary spiral inward in a self-similar way (see Eq. 9). Here the relative gap size, $\lambda = r_g/r_s$, is somewhat decreased after

the gas has accumulated outside the gap, but it is still much larger than the Hill radius.

(iii) An intermediate possibility is that the gap size shrinks over time to within the secondary’s Hill sphere as gas accumulates outside the gap, and eventually closes. The equilibrium steady-state configuration in this continuously overflowing case has an increased density and pressure exterior to the secondary’s orbit (see disk profiles in Fig. 2 for $q \gtrsim 10^{-3}$).

(iv) Finally, it is also possible that the disk becomes geometrically so thick ($H > r$) and/or luminous ($L > L_{\text{Edd}}$) to drive a wind or a three dimensional inflow across the orbit of the secondary.

A necessary condition for the tidal torques to sustain a cavity in the disk is to satisfy $|v_{\text{sr}}| = |v_r(\lambda r_s)|/\lambda$, with the gap closing if and when $|v_{\text{sr}}|$ falls below this value. Here v_{sr} , $v_r(\lambda r_s)$, and λ represent the final steady-state equilibrium values. This condition can be expressed directly with the viscosity in the disk as in Eqs. (21–22), but with the viscosity and scaleheight significantly different from their original values. We utilize the analytic solution to the complete disk model (§ 3.2) as a function of the parameters $(\alpha, \dot{m}, M, f, q, r_s)$ and calculate whether these conditions are satisfied. In practice, we calculate the corresponding range of q and r_s by requiring that the viscous torque at the outer boundary of the near zone be equal to that at the inner edge of the middle zone with a gap assuming unsaturated and saturated tidal torques, respectively (see Paper I for details). This is equivalent to finding q or r_s for gap opening at which the dimensionless angular momentum flux of an overflowing solution becomes first equal to that of the model with a gap. At the gap opening/closing transition $k^{\text{mg}} = \min\{k^{\text{mos}}, k^{\text{mos}}\}$ in Eqs. (11–13). Assuming radiation pressure dominated β disks and negligible GW losses, we find that a truncated disk with an inner cavity forms if

$$q_{\text{u}} \gtrsim 4.7 \times 10^{-3} \alpha_{-1}^{4/3} M_7^{-2/3} f_{-2}^{-4/3} \dot{m}_{-1}^{1/3} r_{s2}^{-1/3}, \quad \text{and} \quad (26)$$

$$r_{\text{ss}} \gtrsim 600 M_{\bullet} \alpha_{-1}^{12/31} f_{-2}^{-4/31} q_{-3}^{3/31} M_7^{-14/31} |\mathcal{W}(-a)|^{-104/155} \quad (27)$$

for unsaturated and saturated tidal torques, respectively (see Eqs. 14–15 for \mathcal{W} and a). Here the first and second conditions are analogous to $\Delta \gtrsim r_{\text{H}}$ (or Eq. 22) and $\Delta \gtrsim H$ (or Eq. 21), respectively, but account for the self-consistent steady-state radial variations in H , Σ , and ν when calculating the viscous and integrated tidal torques for a β disk. Note that Eq. (27) is defined only for $a > 1/e = 0.368$, otherwise the tidal torque is in the unsaturated state. Since a depends on q_s and r_s , Eq. (27) is a nonlinear equation for r_s for a fixed q_s . However, the dependence is logarithmically weak, typically the last factor in Eq. (27) is between 0.3 and 0.8, making the saturated gap-closing radius vary between $(200\text{--}400)M_7 M_{\bullet}$ for all q for the fiducial disk parameters.

As mentioned above, for our overflowing solutions to be physically self-consistent, we must also require $H \lesssim r$ and $L \lesssim L_{\text{Edd}}$, otherwise the radiation pressure would drive an outflow. In § 6, we show that these two conditions are approximately equivalent. Assuming there is a gap, a radiation pressure dominated β disk becomes thick ($H > r$) for mass ratios

$$q_{\text{thick}} \gtrsim 5.4 \times 10^{-3} \alpha_{-1}^{-4/5} \dot{m}_{-1}^{-1} M_7^{6/5} \lambda^{7/2} r_{s2}^3. \quad (28)$$

We find this condition to be less restrictive than $|v_{\text{sr}}| = |v_r|/\lambda$ for unequal masses with $q < 0.1$. The disk does not become geometrically thick if a gap is opened, for our standard disk parameters for $q < 0.1$. The disk thickness is even smaller for radiation pressure dominated α disks implying that overflow occurs before the disk drives a wind in this case too. These conclusions can be understood by setting $H_0/r_s \sim 1$ and $\nu_0 \sim \alpha c_s H \beta^b \sim \alpha H^2 \Omega_s \beta^b \sim \alpha r_s^2 \Omega_s \beta^b$ in the simple gap opening conditions, Eq. (21–22), which implies $q_{\text{thick}} \gtrsim (3k_{\nu 0}/f)^{1/2} \alpha^{1/2} \beta^{b/2}$. Since the constant of proportionality $3k_{\nu 0}/f$ is of order 40 – 50 in the nonlinear regime (Lin & Papaloizou 1986; Crida et al. 2006), there is no secondary mass that satisfies this condition for $\alpha > 0.025$ for an α disk with $b = 0$. We note that Rafikov (2012) arrived at the opposite conclusion using the same argument but setting $3k_{\nu 0}/f \sim 1$, claiming that the disk typically becomes thick and would drive an outflow before the gap may close due to overflow. Furthermore, note that the tidal dissipation effects and the steepening of the angular momentum flux profile $k_{\nu} > k_{\nu 0}$ help further to make the disk prone to overflow before the disk becomes very thick.

The red line in Fig. 4 shows the boundary where the gap remains open in steady-state and where the disk overflows. Remarkably, the gas overflows in steady-state and closes the gap for $q \gtrsim 10^{-4}$ for all binary separations below $1000 M_{\bullet}$, and gaps remain open only for much larger secondary masses.

The gap-closing criteria derived above are independent of the initial conditions of the disk assuming that the disk is strongly perturbed and relaxes to steady-state. However, in Eq. (16) we have shown that this condition does not always hold near the gap-closing boundary and a time-dependent study is necessary for a more accurate description of gap closing. Furthermore, GW-emission becomes more and more efficient for decreasing binary separations. Figure 4 shows regions where GW emission starts to become relevant and where it dominates. In the region marked “gas+GW driven”, the GW-inspiral is slower than the unperturbed viscous accretion speed but faster than the steady-state gas overflow. We did not consider this regime in detail, but Paper I indicates that there may still be a build-up of gas mass, and possibly overflow here, albeit at a slower rate than if GW emission was neglected. In the region marked as “GW inspiral” in Fig. 4, steady-state overflow is prevented by the faster GW-inspiral. In this region, the actual state of the disk depends on the initial condition. If a gap is open when the binary crosses the critical radius where GW-emission becomes dominant, then the gap decouples from the binary and remains empty until the merger. Figure 4 shows that this occurs if the secondary mass is larger than approximately $m_s \gtrsim 4 \times 10^5 M_{\odot}$. For these masses, an X-ray afterglow is activated once the gas refills the gap on the viscous timescale, typically many years after a GW event (Milosavljević & Phinney 2005; Tanaka et al. 2010; Liu & Shapiro 2010; Tanaka & Menou 2010; Shapiro 2010). However, for smaller secondary masses, Fig. 4 shows that the gap overflows and closes before entering the GW inspiral phase. We conclude that a gap may not be present, and significant X-ray emission accompanies the GW-emitting stage for these *LISA/NGO* sources. The EM counterpart may be modulated by the GW-driven binary (Armitage & Natarajan 2002; Chang et al. 2010;

Farris et al. 2011; Bogdanović et al. 2011; Bode et al. 2012; Noble et al. 2012; Baruteau et al. 2012; Giacomazzo et al. 2012; Farris et al. 2012), but future work is necessary to explore this possibility in more detail with initial conditions consistent with the overflowing solution.

5 MIGRATION

The migration rate of the secondary, v_{sr} , follows from Eq. (18), where $\partial_r T_d$ is given in terms of Σ and H using Eq. (4–6) for which we use the steady-state solution derived above. The result can be expressed in terms of the dimensionless angular momentum flux k_s in Eqs. (11–13), as

$$v_{\text{sr}} = -2k_s \frac{\dot{M}r_s}{m_s} - \frac{64}{5} q \bar{r}_s^{-3}, \quad (29)$$

where the first and second terms correspond to disk-driven migration and to GW-driven inspiral, respectively.

Figure 5 shows the gas velocity as a function of radius, and the migration rate of the secondary for the numerical solutions corresponding to Fig. 2. The disk has a gap for $q = 0.1$ and 0.01 when $r_s = 10^3 M_\bullet$, where the nearby gas mass and the secondary move radially at a similar speed. In this case, the secondary and the disk move inwards to maintain a ratio $v_r(\lambda r_s)/v_{\text{sr}} = \lambda$, where λr_s is the characteristic radius where the tidal torque is exerted. The increase of the gas velocity near the gap edge is due to the fact that the steady-state assumption is strongly violated there (see further discussion in § 5.2). At smaller binary separations, the gas can flow across the barrier represented by the secondary, the disk is no longer truncated, and the migration rate is much slower than the gas velocity.

The gas–secondary interaction has a different character when the mass of the secondary is so small that it does not perturb the surface density and scaleheight profile significantly (Type-I), and when it is so large that a gap opens (Type-II). We first discuss these two limiting cases below, and then turn to the intermediate state with a steady-state overflowing disk with a pile-up (which we label “Type-1.5”).

5.1 Type-I migration

Let us first consider a secondary with a mass so small that it makes only a small change in the surface density and scaleheight profile Σ_0 and H_0 and the azimuthal density perturbations are in the linear regime (i.e. $r_H < H$). Here we estimate the corresponding Type-I migration rate using the adopted simple tidal torque model, Eq. (6).¹⁰ For this estimate we extrapolate the torque to within the Hill sphere.

These estimates are included for completeness here, but we emphasize that they are very sensitive to the approximations used in the tidal torque and the disk physics. The true Type-I migration rate (even the sign!) can be significantly different for many reasons including: thermal effects (Paardekooper & Mellema 2006; Paardekooper & Papaloizou 2008), heat diffusion (Paardekooper et al. 2011), inclination (Bitsch & Kley

2011), turbulence and MHD effects (Nelson & Papaloizou 2004; Laughlin et al. 2004), nonlinearities (Dong et al. 2011), resonance overlaps (Rafikov & Petrovich 2012), and gas in horse-shoe orbits (Type-III migration) (Paardekooper et al. 2010). 3D effects for relatively thin disks are less significant (Tanaka et al. 2002).

We assume that near r_s , $\Sigma = \Sigma_s(r/r_s)^{\gamma_\Sigma}$ and $H = H_s(r/r_s)^{\gamma_H}$, where the exponents γ_Σ and γ_H may be slightly different inside and outside the secondary’s orbit due to the tidal effects, $\gamma_{\Sigma,H}^{\text{ni}}$ and $\gamma_{\Sigma,H}^{\text{ne}}$, respectively. For unperturbed disks, $\gamma_H \approx 0$ and $\gamma_\Sigma \approx 3/2$ and $\gamma_\Sigma \approx -3/5$ for α and β disks respectively in the radiation pressure dominated case, while in the gas pressure dominated case $\gamma_H \approx 21/20$ and $\gamma_\Sigma \approx -3/5$ (see Table 1 in Paper I and Eq. (5) in Haiman et al. 2009). Note that the scaleheight gradient can be expressed in terms of the midplane temperature gradient $T_c \propto r^{\gamma_T}$ as $\gamma_H = 3 - \gamma_\Sigma + 4\gamma_T$ for $\beta \ll 1$ and $\gamma_H = \frac{3}{2} + \frac{1}{2}\gamma_T$ for $\beta \sim 1$.

The tidal torque in Eq. (18) can be integrated analytically in powers of the small quantity H/r_s in the four domains of Eq. (6), respectively, where $r > r_s$ or $r < r_s$ (i.e. interior vs. exterior zone) and $\Delta = H$ or $|r - r_s|$ (i.e. saturated vs. unsaturated torque). To first beyond leading order,

$$v_{\text{sr},\text{I},\text{iu}} = +\frac{1}{3}v_{\text{I},-3} - \left(2 + \frac{\gamma_\Sigma^{\text{ni}}}{2} - \gamma_H^{\text{ni}}\right)v_{\text{I},-2}, \quad (30)$$

$$v_{\text{sr},\text{I},\text{is}} = v_{\text{I},-3} - \left(2 + \frac{\gamma_\Sigma^{\text{ni}}}{2} - \gamma_H^{\text{ni}}\right)v_{\text{I},-2}, \quad (31)$$

$$v_{\text{sr},\text{I},\text{es}} = -v_{\text{I},-3} - \left(\frac{\gamma_\Sigma^{\text{ne}}}{2} - \gamma_H^{\text{ne}}\right)v_{\text{I},-2}, \quad (32)$$

$$v_{\text{sr},\text{I},\text{eu}} = -\frac{1}{3}v_{\text{I},-3} - \left(\frac{\gamma_\Sigma^{\text{ne}}}{2} - \gamma_H^{\text{ne}}\right)v_{\text{I},-2}, \quad (33)$$

where we have expressed the results in terms of

$$v_{\text{I},n} = 2\pi f \frac{q}{M_\bullet} \Sigma_s r_s^3 \Omega_s \left(\frac{H_s}{r_s}\right)^n. \quad (34)$$

In particular for unperturbed β -disks,

$$v_{\text{I},-2} = \begin{cases} 440 \text{ cm s}^{-1} \alpha_{-1}^{-4/5} \dot{m}_{-1}^{-7/5} f_{-2} q_{-3} M_7^{6/5} r_{s2}^{29/10} & \text{if } \beta \ll 1, \\ 1.2 \times 10^4 \text{ cm s}^{-1} \alpha_{-1}^{-3/5} \dot{m}_{-1}^{1/5} f_{-2} q_{-3} M_7^{7/5} r_{s2}^{4/5} & \text{if } \beta \sim 1. \end{cases} \quad (35)$$

Thus, all four domains contribute to the migration rate in a nonnegligible way. The total interior and exterior torques are

$$v_{\text{sr},\text{I},\text{i}} = v_{\text{sr},\text{I},\text{iu}} + v_{\text{sr},\text{I},\text{is}} = \frac{4}{3}v_{\text{I},-3} - \left(4 + \gamma_\Sigma^{\text{ni}} - 2\gamma_H^{\text{ni}}\right)v_{\text{I},-2}, \quad (36)$$

$$v_{\text{sr},\text{I},\text{e}} = v_{\text{sr},\text{I},\text{es}} + v_{\text{sr},\text{I},\text{eu}} = -\frac{4}{3}v_{\text{I},-3} - \left(\gamma_\Sigma^{\text{ne}} - 2\gamma_H^{\text{ne}}\right)v_{\text{I},-2}. \quad (37)$$

When combining the torques of the interior and exterior zones, the leading order term, proportional to $v_{\text{I},-3}$, drops out, irrespective of the exponents. This cancellation makes Type-I migration very sensitive to the local disk physics. Denoting average (over the inside and outside near zones)

¹⁰ The tidal torque coefficient in Eq. (6) is $f = 0.80$ in this case, see Goldreich & Tremaine (1980) and Paper I.

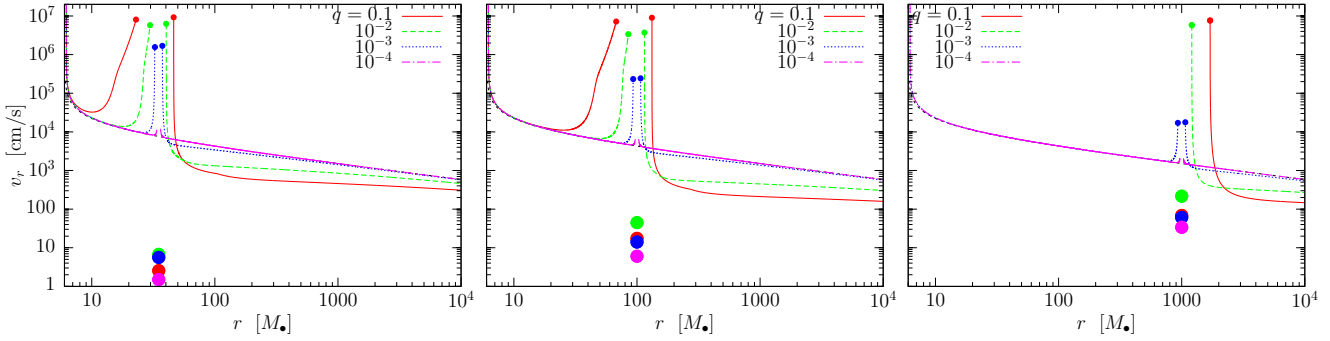


Figure 5. The accretion speed for the disks shown in Fig. 2 and the migration speed of the secondary neglecting GW emission.

quantities by $\bar{\gamma}_\Sigma$ and $\bar{\gamma}_H$,

$$v_{\text{sr},\text{I}} = v_{\text{sr},\text{I},\text{i}} + v_{\text{sr},\text{I},\text{e}} = -(4 + 2\bar{\gamma}_\Sigma - 4\bar{\gamma}_H)v_{\text{I},-2} \quad (38)$$

$$= \begin{cases} -7v_{\text{I},-2} & \text{if } \beta \ll 1, b = 0, \\ -\frac{14}{5}v_{\text{I},-2} & \text{if } \beta \ll 1, b = 1, \\ \frac{7}{5}v_{\text{I},-2} & \text{if } \beta \sim 1. \end{cases} \quad (39)$$

The last equality corresponds to the exponents in unperturbed α and β -disks as given above.

Equation (38) can be understood as follows. The migration rate is a consequence of the opposing repulsive tidal effects of the inner and the outer disks. Since the local disk mass is proportional to $r^2\Sigma \propto r^{2+\gamma_\Sigma}$, the migration rate is directed inward for a constant thickness disk ($\gamma_H = 0$), if and only if the local disk mass increases outward. However, the scaleheight sets the scale at which the torque is suppressed, and acts to reduce the effect. For gas pressure dominated disks, these estimates match the magnitude of the Type-I migration rate of more accurate local torque and hydrodynamical models of Tanaka et al. (2002) and Paardekooper et al. (2010) if $f \sim 0.3$ in Eq. (6) and (34). A different overall offset, mostly due to co-rotation torques and pressure gradient effects, directs the migration inward in those models for a gas-pressure dominated disk. However, recent numerical simulations of non-isothermal optically thick disks with tidal heating find outward migration (Paardekooper & Mellema 2006), and for MHD turbulent disks the sign of the migration oscillates stochastically (Nelson & Papaloizou 2004). This highlights the extreme sensitivity of Type-I migration to subtleties in the disk physics for low-mass secondaries.

5.2 Type-II migration

Next let us consider the limit that the mass ratio is sufficiently large (i.e. more comparable masses), the tidal torque clears a gap such that the nearby gas accretion velocity matches the migration rate of the secondary. If the mass of the secondary is larger than the local disk mass then gas builds up outside the gap, reducing the accretion velocity and increasing the migration rate until the two match. The resulting *secondary dominated Type-II migration* is much slower than the accretion velocity of an unperturbed disk.

Substituting the steady-state viscous torque, T_ν^{mg} from

Paper I in Eq. (18) we get

$$v_{\text{sr},\text{II}} = -\frac{3^{3/4}\alpha^{1/2}\kappa^{1/8}}{2\pi^{1/4}(\mu m_p/k)^{1/2}\sigma^{1/8}} \frac{\dot{M}^{5/8}}{m_s^{3/8}\lambda^{-11/16}\Omega_s^{1/4}r_s^{1/4}} \\ = -550 \frac{\text{cm}}{\text{s}} \alpha_{-1}^{1/2} \dot{m}_{-1}^{5/8} M_7^{1/4} q_{-3}^{-3/8} \lambda^{-11/16} r_{s2}^{1/8}, \quad (40)$$

assuming GW losses are negligible compared to the gas driven migration. Here $1 \lesssim \lambda \lesssim 3$ sets the relative distance to the nearby gas outside the gap responsible for the tidal torque (see Eq. 9). In Paper I we show that depending on whether or not the torque cutoff operates

$$\lambda = \begin{cases} 1 + 0.13 \alpha_{-1}^{-4/37} \dot{m}_{-1}^{4/37} M_7^{-3/37} f_{-2}^{9/37} q_{-3}^{22/37} r_{s2}^{-33/74}, \\ 1 + 0.047 \alpha_{-1}^{-1/3} \dot{m}_{-1}^{-1/12} M_7^{1/6} f_{-2}^{1/3} q_{-3}^{7/12} r_{s2}^{1/12}. \end{cases} \quad (41)$$

The small blue dots in Figs. 6 and 7 show the migration rate of the secondary v_{sr} and the red circles show local gas velocity v_r/λ in the numerical solution of § 3.1 for different q and r_s . The dotted black curves marked as Type-II in Figs. 6 and 7 show that the analytic formula is in excellent agreement with the numerical steady-state solution when a gap forms. Figure 7 shows that the migration rate is reduced relative to the unperturbed disk gas velocity (red curves at $q \rightarrow 0$) at the given radius.

Our result for steady-state Type-II migration, Eq. (40), is consistent with the secondary dominated Type-II migration rate of Syer & Clarke (1995), suppressed by a factor $\lambda^{-11/16} \lesssim 2$. Note that other than \dot{M} and this weak λ dependence, the Type-II migration rate is insensitive to the details of the disk physics and the disk-satellite interaction whenever a gap exists. (In particular to the f coefficient in the tidal torque Eq. (6), the pressure gradient, the thermal state of the disk, and the torque cutoff.) The Type-II migration rate is set by the accretion rate, which is set by the boundary condition, which we assume is a fixed fraction of the Eddington value of the primary.

Further modifications are possible if the disk is not in steady-state. The self-similar solution of Ivanov et al. (1999) (see also Rafikov 2012) leads to a slower migration rate (by another factor ~ 2 relative to Eq. 40). There, the steady-state accretion rate is assumed to hold in the far zone outside the gap and equal to the rate \dot{M}_{Edd} corresponding to the Eddington limit near the primary, but the accretion rate is reduced in the middle zone relative to the steady-state solution, as a fraction of \dot{M} is continuously used to gradually build-up the gas mass outside the gap, which never fully reaches the steady-state level. While these models may be

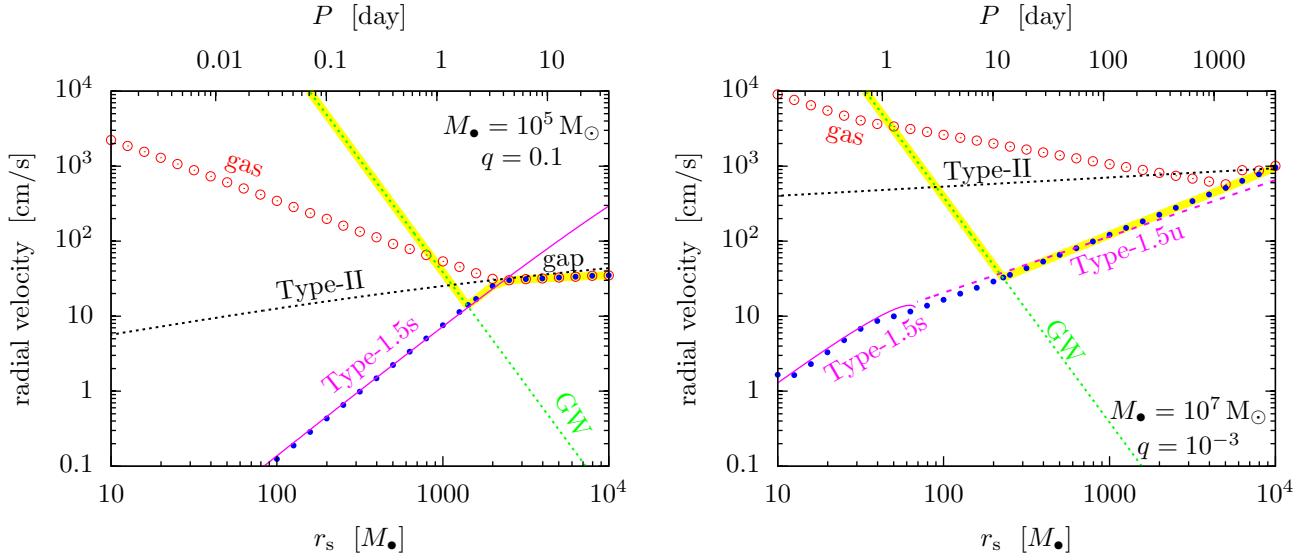


Figure 6. Migration rate of the secondary (small blue bullets), radial velocity of the gas (red circles) from the numerical solution neglecting GW emission for $(M_{\bullet}, q) = (10^5 M_{\odot}, 0.1)$ (left) and $(10^7 M_{\odot}, 0.001)$ (right panel). Analytic migration rates are also shown as labeled (Type-II, 1.5, GW) as a function of orbital radius. The magenta line shows the saturated and unsaturated Type-1.5 migration rates, black dotted line is the Type-II rate. A gap is present when the blue bullets and red circles overlap. The green dotted line shows the GW inspiral rate. The numerical result tracks the analytic Type-1.5 rate when there is no gap. The actual evolutionary sequence of the binary is highlighted with a thick yellow line.

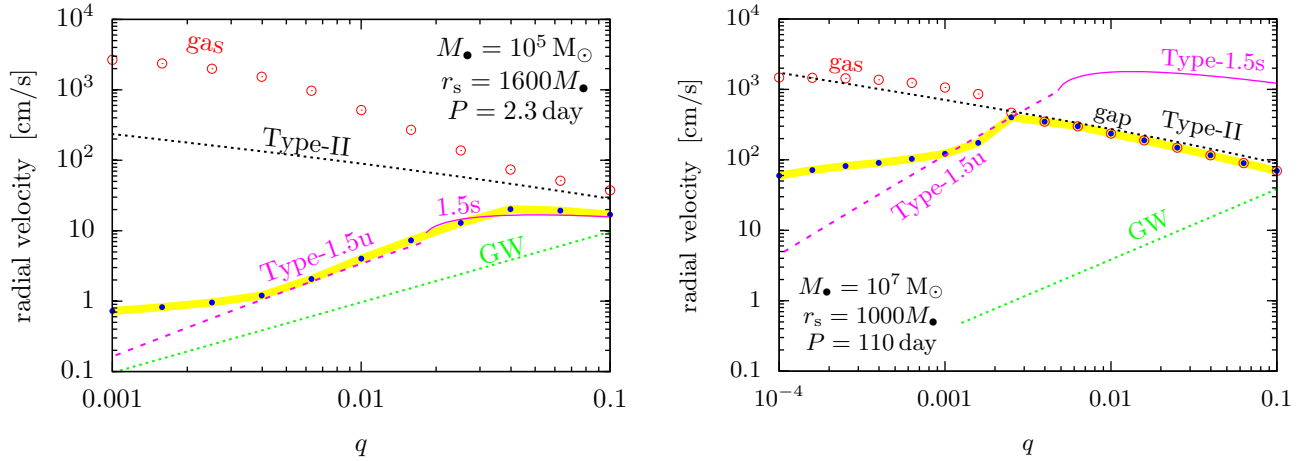


Figure 7. Same as Fig. 6 but varying q at fixed orbital radii.

more realistic, however, there is no strong reason to believe that the far zone accretion rate is related to the Eddington limit of the primary, in a scenario with a gap where the gas is not present in the vicinity of the primary. If one were to assume that \dot{M} is set by the inner boundary condition in the middle zone to a given fraction of \dot{M}_{Edd} , (implying that this may require a correspondingly somewhat larger \dot{M} in the far-zone), this would have led to the original, quasi-steady-state Syer & Clarke (1995) migration rate.

Another possibility was considered in Lodato et al. (2009), in which the total amount of gas mass is limited to be less than the secondary mass, so that the steady-state with \dot{M}_{Edd} cannot be reached. They argued that the migration is much slower in this case, and the disk cannot deliver the secondary efficiently to separations where GW emission

is sufficient to lead to merger in a Hubble time (final parsec problem, see § 5.4).

5.3 Type-1.5 migration

In the previous description, Type-I migration requires azimuthally linear perturbations, which is applicable if $r_{\text{H}} \lesssim H$, implying that $q \lesssim 3(H/r)^3$. By contrast Type-II migration assumes a truncated disk with negligible overflow which is valid if the gap does not close as discussed in § 4. Let us now consider the intermediate Type-1.5 case, when the secondary mass is large enough that its tidal torques cause a significant gas build-up exterior to the secondary orbit but without completely truncating the disk.

The transition between Type-I and II migration as a function of secondary mass was previously investigated ana-

lytically by Hourigan & Ward (1984) and Ward & Hourigan (1989) (see also Ward 1997), numerically by Bate et al. (2003), and in both ways by Crida & Morbidelli (2007), assuming a constant sound speed and viscosity, in cases where the gas pile-up outside the secondary is small. Here we discuss Type-1.5 migration assuming a quasi-steady-state derived in Paper I in the limit of a large pile-up, self-consistently accounting for variations caused by tidal heating, which changes the temperature, scale height, viscosity in the disk.

The migration rate is generally proportional to the dimensionless angular momentum flux in the gas driven regime (Eq. 29). This is sensitive to the nearby gas density and the characteristic radius at which the torque is exerted, $v_{\text{sr}} \propto k \propto \Sigma \Delta^{-3}$, where $\Delta \sim \max(r_{\text{H}}, H)$. If a wide gap forms, Δ is set such that v_{sr} matches the gas inflow rate $v_{\text{sr}} = v_r \propto \dot{M}/\Sigma \propto \nu$ (Type-II). However, in the overflowing case, the migration rate becomes slower than Type-II as the pile-up is limited by gap overflow, decreasing Σ and H compared to the case with a gap. Relative to an unperturbed disk, although Σ is decreased close to the secondary, it is strongly increased due to pile-up outside of Δ . However, more importantly, the pile-up also increases the viscous stress and H , which affects the migration rate greatly as $v_{\text{sr}} \propto H^{-3}$ if $H > r_{\text{H}}$. Accounting for the change in H is essential to correctly estimate the migration rate. The competition of these effects determines the Type-1.5 migration rate in the overflowing regime.

In the self-consistent steady-state overflowing model the migration rate can be obtained by substituting k_{s} from Eqs. (12–13) in Eq. (29). In the torque-saturated state, which is most relevant for a relatively massive secondary, the migration speed is

$$v_{\text{sr},1.5\text{s}} = 23 \frac{\text{cm}}{\text{s}} \alpha_{-1}^{-2/11} f_{-2}^{5/22} q_{-3}^{-6/11} M_7^{23/22} r_{s2}^{83/44} \times |\mathcal{W}(-a)|^{13/11}. \quad (42)$$

In the opposite, torque-unsaturated regime for a relatively low-mass secondary,

$$v_{\text{sr},1.5\text{u}} = 31 \frac{\text{cm}}{\text{s}} \alpha_{-1}^{-2} M_7^{3/2} f_{-2}^{5/2} q_{-3}^{3/2} r_{s2}^{3/4} \left[1 + \frac{\delta r_i}{r_s} \right]^{-35/6}. \quad (43)$$

Here GW emission is assumed to be negligible, appropriate in the zone to the right of the dotted line in the r_s - q plane in Fig. 4 (i.e. large r_s and/or small q). These formulae apply only when the tidal torques generate a sufficiently strong barrier that the surface density of the exterior disk is greatly modified but a gap does not open. This requires r_s and q to fall in the zone marked by “overflow (Type-1.5)” in Fig. 4.

The migration rate is not always Type-1.5 for other choices of q and r_s as shown in Figs. 6 and 7. However, the migration rate is approximated to within 20% by Type-1.5, Eqs. (42–43), for $q \gtrsim 10^{-3}$ and $r_s \gg r_{\text{ISCO}}$ whenever a gap is not present and GW emission is negligible, provided that the disk is in a quasi-steady state and the torque model is given by Eq. (6). These formulae capture the (q, r_s) parameter dependence remarkably well in this range, where the Type-I and II rates are inapplicable. Note, however, that since our results, Eqs. (42–43), correspond to the case of a large pile-up, this is insufficient to investigate very small

mass ratios where the transition between the Type-I and 1.5 regimes takes place.

Figures 6 and 7 show that Type-1.5 migration is generally slower than the other velocity scales in the problem. Increasing the secondary mass at a fixed orbital radius generally increases the amount of gas mass accumulated outside the secondary, which causes the gas velocity to be reduced for a fixed accretion rate. However, since there is no gap in the disk, gas still flows in faster than the migration rate of the object. Type-1.5 migration is slower than the secondary-dominated Type-II migration rate, since the gas pileup in these overflowing solutions just outside the orbit is less pronounced compared to the case with a gap. Finally, it is also slower than the Type-I rate if the tidal torques decrease the gas density close to the secondary or if the scaleheight is increased.

5.4 GW driven inspiral

As the separation decreases, the rate of energy and angular momentum loss associated with GW emission increases rapidly. The GW-inspiral speed (from the standard quadrupole formula for GW emission, Peters 1964) is

$$v_{\text{sr}}^{\text{GW}} = -\frac{64}{5} q r_s^{-3}. \quad (44)$$

This is shown by a green dotted line in Figs. 6 and 7. Unlike Type-I, Type-1.5, or Type-II migration, the GW inspiral velocity increases toward smaller separations. The GW inspiral timescale is larger than the Hubble time at large separations, where the evolution is driven by the gaseous disk. Gas may be responsible for delivering binaries to the separations corresponding to the GW-driven regime (but see discussion in § 5.2). Gas-driven migration may transition to the GW-driven regime either in the presence of a gap for comparable mass binaries for $M \gtrsim 10^7 M_{\odot}$, or in the overflowing state for smaller mass ratios and/or total masses (see Fig. 4).

5.5 Summary of migration rates

We can now summarize and interpret the trends seen for different mass ratios and radii in Figs. 6 and 7. At sufficiently large radii, a gap opens for comparable mass ratio binaries. As gas accumulates outside the gap, the radial gas velocity is slowed down to match the migration rate of the secondary, according to Type-II migration. For smaller secondary masses in this regime, the amount of accumulated gas is less and the corresponding gas accretion velocity becomes higher and the migration rate faster. At sufficiently small secondary mass and binary separation, the tidal torque cannot keep the gas outside the Hill sphere and the gap closes. The gas accretion velocity in this regime is still far slower than the unperturbed value, and the pressure and gas density are significantly enhanced outside the orbit. The migration here is well approximated by the Type 1.5 rate given by Eqs. (42–43). The secondary tends to decrease the surface density and pressure within the Hill sphere relative to the unperturbed value. The migration rate approaches the Type-I rate from below for very small q . Along the inward migration of the binary, the amount of local gas mass torquing the binary decreases. This implies that the migration rate decreases with decreasing radius for all three

cases (Type-I, 1.5, and II). GW emission dominates over gas driven migration in the final stages before merger.¹¹

6 OBSERVATIONAL IMPLICATIONS

6.1 Bolometric luminosity

The total luminosity of the disk is comprised of the viscous and the tidal heating. The energy loss corresponding to inward migration appears as an extra source of heat in the disk, which leads to the brightening of the disk. If the disk is radiatively efficient up to an inner radius r_{\min} , then the emitted luminosity corresponds to the energy loss¹²

$$L = \frac{1}{2} \frac{GM_{\bullet} \dot{M}}{r_{\min}} - \frac{1}{2} \frac{GM_{\bullet} m_s}{r_s^2} (v_{\text{sr}} - v_{\text{sr}}^{\text{GW}}) \quad (45)$$

$$= \frac{\dot{M} c^2}{2 \bar{r}_{\min}} - \frac{1}{2} \frac{c^5}{G} \frac{q}{\bar{r}_s^2} \frac{v_{\text{sr}}}{c} + \frac{32}{5} \frac{c^5}{G} \frac{q^2}{\bar{r}_s^5} \quad (46)$$

where $\bar{r} = r/(Gc^{-2}M_{\bullet})$ and v_{sr} is the migration rate due to gas and GW losses ($v_{\text{sr}} < 0$ for inward motion), and $v_{\text{sr}}^{\text{GW}}$ is the GW inspiral rate neglecting torques from the gas. The first term is due to accretion, the second and third terms together are due to tidal heating, labeled L_{acc} and ΔL_{heat} below, respectively.

Figure 8 shows the two components of the luminosity L_{acc} and ΔL_{heat} relative to $\dot{M}c^2$ as a function of the binary orbital time when neglecting GW emission. Here we assume that $\dot{M}c^2 = L_{\text{Edd}} = 1.4 \times 10^{45} M_7 \text{ erg/sec}$ where $M_7 = M/10^7 M_{\odot}$. The point and line styles are the same as in Figs. 6 and 7 in the various regimes of migration. The figure shows that the secondary can greatly modify the luminosity of the disk. The accretion luminosity is greatly decreased if a gap forms, but the excess brightness of the outer disk, ΔL_{heat} , can overcompensate for the decrease of L_{acc} .

The analytic results for the migration rates in § 5 can be used to understand the features shown in Figure 8. If a gap is opened and the secondary exhibits Type-II migration, then the luminosity associated with accretion scales with the orbital period P as $L_{\text{acc,II}} \propto 1/r_s \propto P^{-2/3}$ and the secondary causes an excess $\Delta L_{\text{heat,II}} \propto q^2 v_{\text{sr,II}}/r_s^2 \propto q^{13/8} r^{-15/8} \propto q^{13/8} P^{-5/4}$. In the GW-driven regime before gap decoupling, the accretion luminosity is the same but the excess tidal heating rate is negligible. At smaller separations the accretion luminosity increases, and reaches $\dot{M}c^2/(2r_{\text{ISCO}})$ as the gap closes. As the binary becomes GW-driven at smaller separations the gas build-up is decreased outside of the secondary and the excess heating is suppressed. This transition happens in the region marked as gas+GW driven in Figs. 4; at orbital periods $P \lesssim (81, 14, 10)$ days for $q =$

(0.1, 0.01, 0.001), respectively, for $M_{\bullet} = 10^7 M_{\odot}$ in particular. Once the gap closes, r_{\min} is associated with the ISCO, and the accretion luminosity is constant. The tidal heating in the overflowing state is $\Delta L_{\text{heat,1.5}} = q^2 v_{\text{sr,1.5}}/r^2 \propto q^{7/2} r^{-5/4} \propto q^{7/2} P^{-5/6}$ in the unsaturated Type-1.5 state, and $q^{16/11} r_s^{-5/44} \propto q^{16/11} P^{-5/66}$ in the saturated case. For weakly perturbed disks where the secondary undergoes Type-I migration, $\Delta L_{\text{heat,I}} = q^2 v_{\text{sr,I}}/r_s^2 = q^3 r^{9/10} = q^3 P^{3/5}$ in the radiation pressure dominated regime and $q^3 r^{-6/5} = q^3 P^{-12/15}$ in the gas pressure dominated regime.

Figure 8 shows that in some cases $\Delta L_{\text{heat}} \sim L_{\text{Edd}}$. In this case, the disk near the secondary becomes brighter than the inner accretion disk, so that the disk appears moderately super-Eddington. While this may appear contradictory, we demonstrate that this does not violate the local Eddington flux limit (Abramowicz et al. 1980; Tanaka & Menou 2010). As shown in § 2, the disk flux can be obtained directly from the temperature and the opacity of the disk. If the disk is supported vertically by gas and radiation pressure, this can be expressed in terms of the disk scaleheight. Assuming that the sound speed satisfies $H = c_s/\Omega$, the flux is given by $F = (c/\kappa)H\Omega^2(1 - \beta)$ (see Paper I). For a nearly Keplerian thin disk, the integrated flux from the two faces is then

$$L = \frac{4\pi GM_{\bullet} c}{\kappa} \int_{r_{\min}}^{r_{\max}} (1 - \beta) \frac{H}{r} \frac{dr}{r}. \quad (47)$$

Here the first factor outside the integral can be identified as the Eddington luminosity L_{Edd} for a source in hydrostatic equilibrium, while the integral is a geometrical factor which is less than unity for a thin disk truncated at the ISCO. For a stationary accretion disk without a secondary, $H(r)$ is a constant in the most luminous, radiation pressure dominated regime ($\beta \approx 0$), and the integral reduces to $L = \dot{M}c^2/(2\bar{r}_{\min})$. More generally, $L = \eta \dot{M}c^2 = \epsilon L_{\text{Edd}}$. In Fig. 8, we conservatively chose $\bar{r}_{\min} = 6$ corresponding to a non-spinning BH, and $\epsilon = \eta$ consistent with AGN observations showing that $\epsilon \sim 10\%$ – 25% for bright AGNs (Kollmeier et al. 2006; Trump et al. 2009). The luminosity increase due the secondary is significant if H/r is larger near the secondary than near the ISCO and if the disk is radiation pressure dominated. Indeed, Fig. 2 has shown that H/r can increase dramatically for $q > 10^{-3}$. Eq. (47) shows that a thick, radiation pressure dominated accretion disk can exceed the hydrostatic Eddington limit by a logarithmic factor, $\ln(r_{\max}/r_{\min})$. This is due to the velocity shear and vorticity in the disk, which are neglected in the hydrostatic Eddington limit (Abramowicz et al. 1980; Abramowicz 2004).

We conclude that the disk luminosity may be modified significantly by the orbiting object. Whenever a gap forms, the disk becomes either fainter due to the loss of accretion onto the primary or brighter due to the accumulated gas mass outside the secondary heated by tidal dissipation (with the latter effect dominating near the end of the Type II migration phase in many cases). The competition of these effects generates a unique lightcurve which is sensitive to the type of migration as well as to GW losses. These conclusions assume axisymmetry; an obvious caveat is that non-axisymmetric accretion streams could generate significant luminosity (Hayasaki et al. 2008; Roedig et al. 2011, 2012).

¹¹ A separate class of migration for low-mass planets, which we did not consider here is Type-III migration associated with torques exerted by the gas on horseshoe orbits around the secondary (Masset & Papaloizou 2003). This is significant if the gas mass is considerable relative to the secondary mass. Although the secondary mass dominates over the local disk mass for BH binaries embedded in accretion disks of interest here, future studies should investigate the effects of the gas crossing the secondary orbit (see the recent study by Roedig et al. 2012 for the importance of torques due to gas streams in the central cavity around a SMBH binary).

¹² We include factors of G and c in this section.

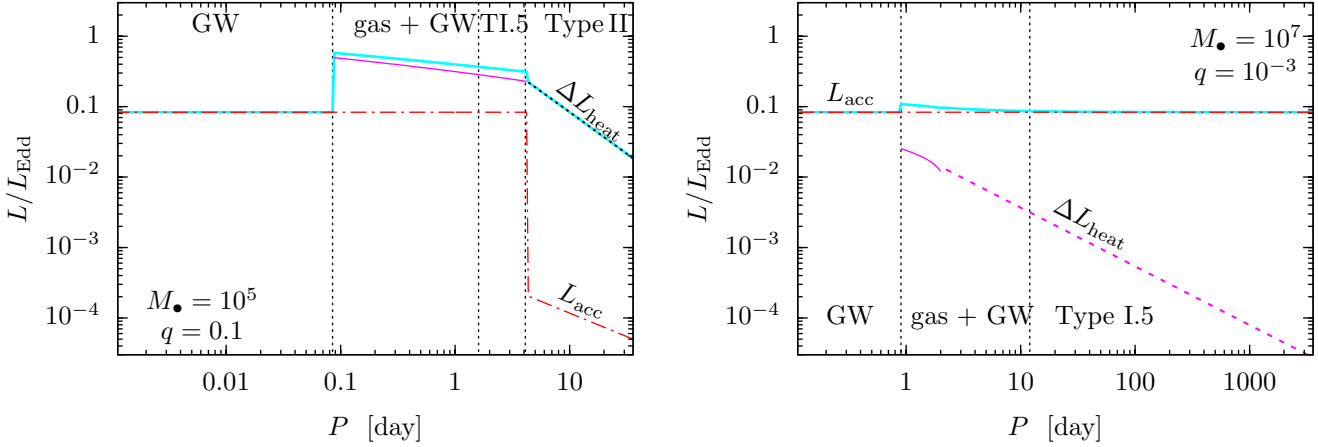


Figure 8. The bolometric luminosity corresponding to accretion and tidal heating as a function of the orbital period of the secondary for $(M_\bullet, q) = (10^5 M_\odot, 0.1)$ and $(10^7 M_\odot, 10^{-3})$ in the various evolutionary stages. The line styles for ΔL_{heat} are the same as in Fig. 6: black dotted for Type-II migration, solid and dashed magenta for saturated and unsaturated Type-1.5 migration. The cyan line shows the total bolometric luminosity $L_{\text{acc}} + \Delta L_{\text{heat}}$. Note that our calculations for ΔL_{heat} neglects GW emission, it breaks down in the GW-inspiral regime. L_{acc} is quenched when a gap opens.

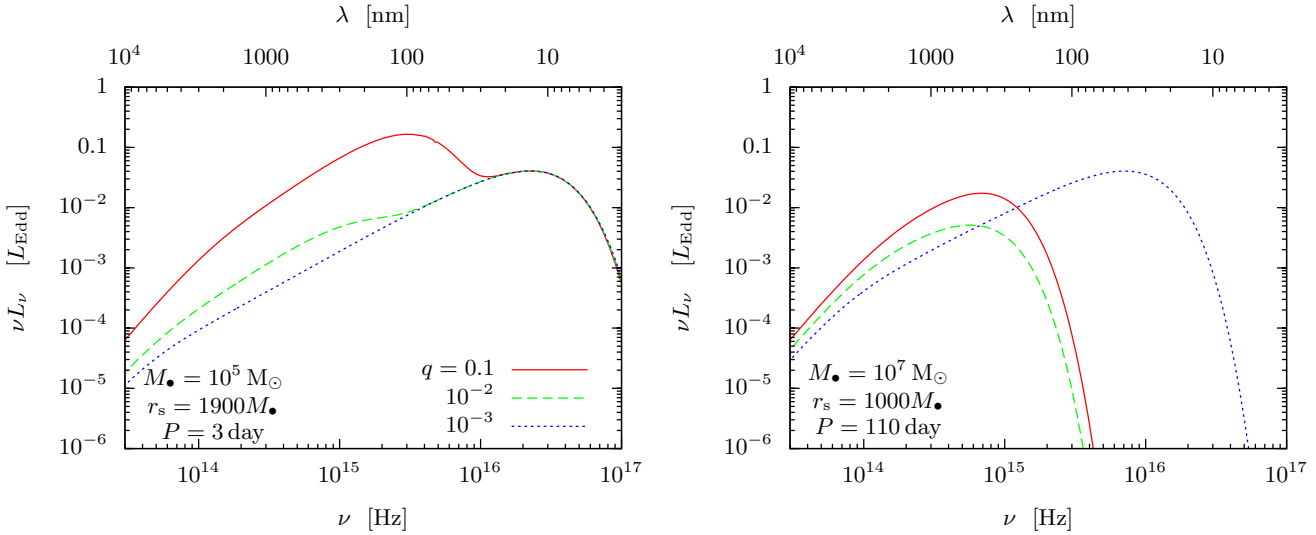


Figure 9. Disk spectra in units of $L_{\text{Edd}} \sim 10^{43}$ and 10^{45} erg/s for $M_\bullet = 10^5$ and $10^7 M_\bullet$ binaries with periods as marked. Different curves correspond to different mass ratios as labeled. The dotted curve ($q = 10^{-3}$) represents the asymptotic spectrum of a solitary disk. The spectrum on the right panel is truncated for $q = 0.1$ and 0.01 when a gap forms. The optical enhancement at lower frequencies is due to the outer disk.

6.2 Disk spectrum

We obtain a simple estimate of the disk spectrum by assuming multicolor black body radiation for each annulus with the given surface temperature profile $T_s(r)$,

$$B(\nu, T) = \frac{2h\nu^3}{c^2} \frac{1}{e^{h\nu/kT} - 1} \quad (48)$$

and integrating over radius

$$L_\nu = 4\pi^2 \int_{r_{\text{min}}}^{r_{\text{max}}} B[\nu, T_s(r)] r dr. \quad (49)$$

We ignore gravitational redshift and Doppler boost for simplicity since $\bar{r} \gg 1$ (however, see discussion below).

The outer parts of the accretion disk have a much lower temperature than the inner parts. Therefore, the brighten-

ing caused by a secondary affects the spectrum more prominently at shorter wavelengths. The disk spectrum can be used to disentangle the effects of a secondary from the properties of the inner disk.

Figure 9 shows the disk spectra in two representative cases when the orbital period is $P = 3$ or 110 days for $M_\bullet = 10^5$ and $10^7 M_\odot$, respectively. Different curves show different mass ratios. The spectrum is truncated at high frequencies when a gap forms, as the hottest central regions are removed from the disk. Relative to an accretion disk with no secondary, the disk is much brighter in the ultraviolet, optical, and infrared bands for large secondary masses, both in the gap forming and in the overflowing cases. The extra energy originates from the orbital energy of the binary which heats the disk through the gravitational torques on

top of the viscous heating. For other binary masses and separations assuming the binary is in the gas driven regime, the dimensionless angular momentum flux or brightening factor is shown in Fig. 3. For smaller binary separations when the GW inspiral overtakes the accretion rate, the optical and infrared enhancement associated with the exterior gas pileup goes away.

Note that our estimates neglect accretion onto the secondary which can generate an additional spectral peak in X-rays (Sesana et al. 2012; Tanaka et al. 2012). We also neglected relativistic corrections to the disk spectrum, and other features such as spectral lines and the high-frequency tail associated with the corona. Since the orbital velocity of the secondary on a circular orbit is $v_{\text{orb}} = 3 \times 10^4 \text{ km s}^{-1} r_2^{-1/2}$, the offset and broadening of spectral lines can be quite significant for SMBH binaries (Haiman et al. 2009; Shen & Loeb 2010; Dotti et al. 2012; McKernan et al. 2012). Thus, the actual AGN binary spectra shown in Fig. 9 may also exhibit relativistically broadened and/or offset spectral lines by 6,900 and 9,500 km s^{-1} in the left and right panels, respectively. The lightcurve is expected to be periodically modulated on the binary orbital period (3 and 110 days respectively in the two panels; see also discussion below), with harmonics appearing at ~ 3 and 0.5 times the orbital period for mass ratios $q \gtrsim 0.05$ (D’Orazio et al. 2012, in preparation). These signatures together can help future observational efforts to identify SMBH binaries in the overflowing regime.

6.3 Transient and periodic variability statistics

We have calculated the rate at which the binary evolves toward merger and have shown that the state of the disk changes during this process. From this one can predict the residence time $t_{\text{res}} \equiv r/v_{\text{sr}}$ the binary resides in the various states. Assuming that the luminosity of the accretion disk is modulated periodically on the orbital timescale (Hayasaki et al. 2007; MacFadyen & Milosavljević 2008; Cuadra et al. 2009), it is possible to predict the relative fraction of binaries that exhibit variability as a function of orbital period (Haiman et al. 2009). One may expect to see EM transients when the binary is surrounded by gas, and a different distinct population of dimmer or softer sources decoupled from the disk assuming that the GW inspiral dominates the evolution inside of a gap in the disk. The predictions can be observationally tested using large deep variability surveys, such as PanSTARRS or LSST.

Previously, Haiman et al. (2009) has carried out this exercise assuming a GW inspiral at short periods and Type-II migration for long periods. These predictions have to be revised in two respects. First, many of the binaries may be in the Type-1.5 regime which has a longer residence time. Second, we predict that tidal torques cannot sustain a gap once a sufficient amount of gas has accumulated, which may cause gap-refilling, before the binary can “run away” from the gap edge in the GW-driven inspiral regime. Without gap-refilling or an inner disk around the primary and secondary, periodic variability is not expected in the GW-driven regime with a decoupled outer disk (see however Farris et al. 2011; Bode et al. 2012; Noble et al. 2012; Farris et al. 2012). Future studies should investigate the expected variability in

circumbinary or overflowing disks, where the secondary is in the GW-driven regime.

Figure 10 shows the residence time the binary spends at various orbital periods for different masses and mass ratios. Different line styles show the type of migration. The residence time increases with period very quickly ($t_{\text{res}} \propto t_{\text{orb}}^{8/3}$) in the GW driven regime, but not so rapidly in the gas driven regime. The dependence is flatter for Type-II, and even more so for Type-1.5, where it can even decrease with period in the torque-cutoff state (at $P \sim 1$ day for $10^5 M_{\odot}$ in the right panel). This shows that the efficiency at which gas can deliver objects to the GW driven regime is deteriorated by gas overflow. The transitions to GW-driven inspiral occurs at longer periods for the Type-1.5 than for Type-II migration (see Fig. 6). The fraction of binaries at orbital periods between a few days to years is larger if Type-1.5 migration operates, relative to the Type-II rate. As a rule of thumb, we find this to be the case if one of the black holes is less massive than $10^5 M_{\odot}$. Conversely, the residence time follows the Type-II rate all the way to the GW inspiral regime if both objects are more massive than $10^5 M_{\odot}$.

Gap refilling may be witnessed through the increase in the bolometric luminosity and spectral X-ray hardening of the source (Milosavljević & Phinney 2005; Tanaka et al. 2010). Our results show that this may occur already before merger, particularly for $10^5 M_{\odot}$ SMBH masses in the *LISA/NGO* range (Sesana et al. 2005), generating bright electromagnetic sources coincident with GWs. Gap refilling may occur more rapidly compared to the viscous time without the pile-up, due to the enhanced gas mass and stress outside the gap and the presence of the secondary, implying a larger population of birthing quasars for all-sky optical (e.g. LSST) or soft X-ray surveys. However, since this occurs at larger radii where the viscous time is longer, it is unclear whether this yields a larger or smaller population of birthing quasars with significant brightening during the mission lifetime of all-sky optical (e.g. LSST) or soft X-ray surveys.

The significant excess flux in the gas driven regime may increase the prospects for identifying SMBH binary sources. Future surveys for these sources can provide observational evidence for SMBH mergers in the *NGO* mass range or IMBHs orbiting around SMBHs.

6.4 Gravitational wave measurements

Gap refilling and Type-1.5 migration has implications for GW measurements in several ways. First, we have shown that the gap closes much earlier than previously thought. This implies that the *LISA/NGO* binaries may be embedded in gas even for nearly comparable mass ratios. This helps the prospects of identifying coincident EM counterparts to *LISA* sources. Second, the effects of gas may be identified directly from the GW signal itself. The GWs emitted by SMBH binaries is in the frequency bands detectable by pulsar timing arrays (PTAs) if the orbital period is between a few days to a few years, and in the planned *LISA* range if it is between a few seconds to a \sim half day. Figure 10 shows that the corresponding mass range is below $10^6 M_{\odot}$ for *LISA* and above $10^7 M_{\odot}$ for PTAs. Here we describe how the accretion disk affects the GW signal for *LISA* and PTAs, and discuss the implications of gas overflow and Type-1.5 migration.

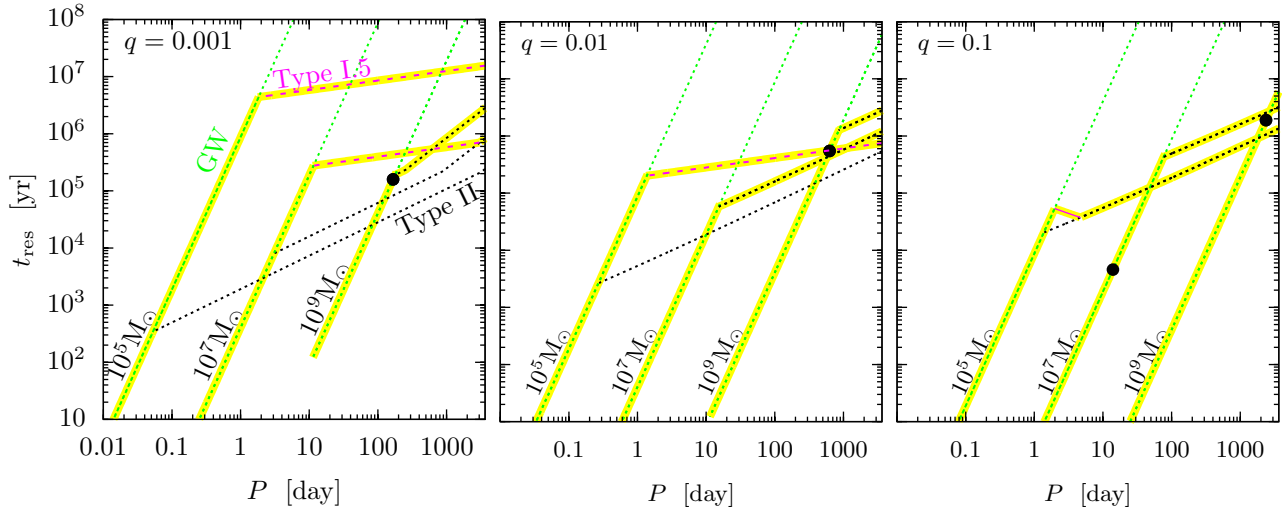


Figure 10. The amount of time the binary spends at various orbital periods during its evolution towards merger. The three panels show different mass ratios, and in each panel the three sets of curves show different total masses as marked. For each mass, different line styles correspond to different types of migration, GW inspiral (green), saturated and unsaturated Type-1.5 (magenta dashed and solid), and Type-II (black dotted). The evolutionary tracks are highlighted with a thick yellow line. Big black dots mark gap decoupling; for much smaller periods, the tidal torques may not generate EM variability.

6.4.1 PTAs

The nHz GW background, measurable by PTAs, is generated by SMBH binaries (Sesana et al. 2008, 2009), which emit a stationary signal with angular frequency 2Ω for circular sources and many distinct upper harmonics for eccentric sources. The background is affected by the disk in two ways: (i) by changing the relative fraction of binaries at particular orbital radii according to the residence time (Kocsis & Sesana 2011), and (ii) by changing the eccentricity distribution of sources if a gap is opened (Artymowicz 1992; Armitage & Natarajan 2005; Cuadra et al. 2009; Roedig et al. 2011, 2012).

Kocsis & Sesana (2011) calculated the GW background for a population of binaries that undergo Type-II migration in steady-state α or β disks, or the self-similar migration according to the quasi-stationary model in Ivanov et al. (1999). They found that the unresolved GW background is typically not reduced significantly in the PTA frequency band if the sources undergo secondary dominated Type-II migration.¹³ This is due to the fact that the background is dominated by comparable mass binaries for which (1) the slowdown of Type-II migration in the secondary dominated regime is more significant and (2) many of these sources transition to a GW dominated evolution at large orbital periods outside the PTA range. Regarding the individually resolvable GW sources with PTAs, they are typically the most massive $q \sim 1$, $\sim 10^9 M_\odot$ binaries, which are not affected by gas in any case at these frequencies. Figure 10 shows that Type-1.5 migration in β -disks is not relevant for PTA measurements since it does not affect the binaries with masses larger than $10^6 M_\odot$. Since gaps are expected not to close for these masses for β -disks, these sources are expected to exhibit GW spectra characteristic of eccentric sources. Further

studies should examine whether gap overflow may occur for PTA sources embedded in α disks, and the implications for eccentricity.

6.4.2 LISA/NGO

As mentioned above, the frequency range of *LISA/NGO* corresponds to binary orbital periods shorter than a day, the sensitivity is best for $P \sim 10$ min. In this regime, the binaries are typically already in the GW inspiral regime. Nevertheless, the effects of gas are imprinted on the frequency and phase evolution of the signal as the orbital period shrinks during the measurement. In Kocsis et al. (2011) and Yunes et al. (2011), we have shown that the corresponding GW phase perturbation is very significant (~ 1000 rad/yr) relative to the *LISA* measurement accuracy (~ 1 rad/yr) if the gaseous torque corresponds to secondary dominated Type-II migration (particularly for $M_\bullet = 10^6 M_\odot$), and less pronounced (~ 10 rad/yr) but still significant if it corresponds to Type-I migration. Here we have not examined the gaseous torques in the GW-driven regime. In that case, since the viscous inflow is slower than the GW-inspiral, the gas does not bank-up outside of the secondary.¹⁴ Therefore, we conclude that gas effects are expected to be reduced compared to the Type-II case in Yunes et al. (2011), but future studies should examine whether the corresponding phase shift is still measurable with the *LISA* accuracy.

The GW spectrum may also be affected by the binary eccentricity, reminiscent of gas (Armitage & Natarajan 2002). We have shown that the disk overflows for typical *LISA* binaries. Further studies should investigate whether the eccentricity is excited in the overflowing state, and

¹³ The background could be reduced only if Type-II migration occurs on the viscous timescale with no accumulation of gas.

¹⁴ Gas may bank up interior to the orbit in the GW driven regime (Chang et al. 2010), see however Baruteau et al. (2012) and § 1.2 above.

whether this remains significant in the GW inspiral regime when the binary enters the *LISA* frequency range.

7 CONCLUSIONS

We have examined the self-consistent steady-state structure of accretion disks around SMBH binaries, conditions of gap closing, and migration rates of the binaries. Our main conclusions can be summarized as follows.

(i) *Gap closing*— The secondary represents a strong tidal barrier in the accretion disk, which causes a significant accumulation of gas in an extended range outside of the secondary. Still, the tidal torque cannot counteract the enhanced viscous torque in steady-state for a large range of binary masses, particularly for $\lesssim 10^5 M_\odot$, and the disk does not form a gap. The steady-state exhibits continuous overflow across the orbit.

(ii) *Phase diagram*— The disk is described by separate formulas in the two main regions in the binary parameter space when GW emission is negligible: A gap is present for sufficiently large separations and masses (Fig. 3) but typically refills before GW-driven decoupling. We identify further sub-regions in this “phase space” depending on whether the tidal torques are saturated.

(iii) *Type 1.5 migration*— The gas-driven migration rate is Type-I for weakly perturbed disks, Type-II where the gap can remain open, and Type-1.5 in the intermediate strongly perturbed inflowing state. We have derived analytic formulas for the Type-1.5 rates and have found these to be slow compared to both Type I and II rates.

(iv) *optical and infrared excess*— The disk flux is increased by a factor of up to 100–500 due to gas pileup outside the orbit of the secondary for binaries with $M_\bullet = 10^5$ – $10^7 M_\odot$ in the Type-1.5 and Type-II migration regimes, enhancing the ultraviolet, optical, and near infrared brightness of the disk. The enhancement is more pronounced for lower M_\bullet . The disk can become moderately super-Eddington at these frequencies. The excess brightness is mitigated by gas overflow and further suppressed for binaries for which GW-emission is significant. This can be used to indirectly indicate the presence of GWs.

(v) *Periodically variable AGN*— The orbital period is between 1 day and 10 years for binaries in the Type-1.5 migration regime. Periodic variability surveys of AGNs can discover these sources and test the predicted spectral signatures. The statistics of the relative abundance of many such sources with different periods can be used to observationally test the migration and GW inspiral rate, and to estimate the expected *LISA* merger rate.

(vi) *EM counterparts for LISA*— The masses most affected by gap overflow and Type-1.5 migration is in the *LISA* range (near $\sim 10^5 M_\odot$). The gap closes even for comparable mass ratios before GW emission dominates, implying that normal AGN-like activity may be coincident with *LISA* sources (Kocsis et al. 2006).

(vii) *PTA sources*— The gap can remain open for the massive 10^8 – $10^9 M_\odot$ binaries, implying that the GW background is not affected by Type-1.5 migration for PTAs. The presence of gas can be inferred either from EM surveys or indirectly from the GW spectrum, since the gas increases

the binary eccentricity if a gap is open, which adds orbital harmonics to the spectrum. The eccentricity is expected to be much smaller for systems devoid of gas (Sesana 2010; Preto et al. 2011; Madigan & Levin 2012).

(viii) *Star formation and final parsec problem*— Previously, Lodato et al. (2009) argued that the migration rate is greatly reduced by star formation feedback if the disk is unstable to gravitational fragmentation and the disk mass is smaller than the secondary mass. However, for the low-mass, but continuously replenished disks considered here we find that the disk is stabilized against gravitational fragmentation. This is because viscous heating increases the sound speed over a large range of radii outside the secondary’s orbit, and this effect is more important than the increase of surface density in the same region.

We note that all of these findings correspond to a disk model in which the effective viscosity is proportional to the gas pressure in the disk (so-called β -disks). Future studies should investigate alternative models in which the viscosity is proportional to the total gas+radiation pressure. We also assumed steady-state models, where the accretion rate is constant, and set by the Eddington limit of the primary. While we expect these assumptions to be justified in the overflowing regime, where the gas inflow rate is much higher than the migration rate of the secondary, the steady-state Eddington accretion assumption is suspect for circumbinary disks with gaps (Ivanov et al. 1999; Lodato et al. 2009; Rafikov 2012). Future studies should address comparable mass binaries where the disk may be significantly non-axisymmetric (MacFadyen & Milosavljević 2008; Cuadra et al. 2009) and where the accretion of the secondary is non-negligible (Lubow et al. 1999), and examine whether binary eccentricity is excited in the overflowing steady-state (Artymowicz 1992; Armitage & Natarajan 2005; Hayasaki 2009; Roedig et al. 2011, 2012).

ACKNOWLEDGMENTS

We thank Re’em Sari, Taka Tanaka, Roman Rafikov, and Alberto Sesana for useful discussions. BK acknowledges support from NASA through Einstein Postdoctoral Fellowship Award Number PF9-00063 issued by the Chandra X-ray Observatory Center, which is operated by the Smithsonian Astrophysical Observatory for and on behalf of the National Aeronautics Space Administration under contract NAS8-03060. This work was supported in part by NSF grant AST-0907890 and NASA grants NNX08AL43G and NNA09DB30A (to AL) and NASA grant NNX11AE05G (to ZH).

REFERENCES

- Abramowicz M. A., 2004, ArXiv e-print astro-ph/0411185
- Abramowicz M. A., Calvani M., Nobili L., 1980, ApJ, 242, 772
- Amaro-Seoane et al. 2012, e-print arXiv:1201.3621
- Armitage P. J., 2007, ArXiv e-print astro-ph/0701485
- Armitage P. J., Natarajan P., 2002, ApJ, 567, L9
- Armitage P. J., Natarajan P., 2005, ApJ, 634, 921
- Artymowicz P., 1992, PASP, 104, 769

- Artymowicz P., Lubow S. H., 1994, *ApJ*, 421, 651
- Artymowicz P., Lubow S. H., 1996, *ApJ*, 467, L77+
- Baruteau C., Ramirez-Ruiz E., Masset F., 2012, *MNRAS*, p. L436
- Bate M. R., Lubow S. H., Ogilvie G. I., Miller K. A., 2003, *MNRAS*, 341, 213
- Begelman M. C., Blandford R. D., Rees M. J., 1980, *Nature*, 287, 307
- Bitsch B., Kley W., 2011, *A&A*, 530, A41
- Bode T., Bogdanović T., Haas R., Healy J., Laguna P., Shoemaker D., 2012, *ApJ*, 744, 45
- Bogdanović T., Bode T., Haas R., Laguna P., Shoemaker D., 2011, *Classical and Quantum Gravity*, 28, 094020
- Chang P., Strubbe L. E., Menou K., Quataert E., 2010, *MNRAS*, 407, 2007
- Crida A., Morbidelli A., 2007, *MNRAS*, 377, 1324
- Crida A., Morbidelli A., Masset F., 2006, *Icarus*, 181, 587
- Cuadra J., Armitage P. J., Alexander R. D., Begelman M. C., 2009, *MNRAS*, 393, 1423
- D'Angelo G., Henning T., Kley W., 2003, *ApJ*, 599, 548
- Dong R., Rafikov R. R., Stone J. M., 2011, *ApJ*, 741, 57
- Dotti M., Sesana A., Decarli R., 2012, *Advances in Astronomy*, 2012
- Escala A., Larson R. B., Coppi P. S., Mardones D., 2005, *ApJ*, 630, 152
- Farris B. D., Gold R., Paschalidis V., Etienne Z. B., Shapiro S. L., 2012, *ArXiv e-prints*
- Farris B. D., Liu Y. T., Shapiro S. L., 2011, *Phys. Rev. D*, 84, 024024
- Giacomazzo B., Baker J. G., Miller M. C., Reynolds C. S., van Meter J. R., 2012, *ArXiv e-prints*
- Goldreich P., Goodman J., Narayan R., 1986, *MNRAS*, 221, 339
- Goldreich P., Tremaine S., 1980, *ApJ*, 241, 425
- Goldreich P., Tremaine S., 1982, *ARA&A*, 20, 249
- Goodman J., Tan J. C., 2004, *ApJ*, 608, 108
- Haiman Z., Kocsis B., Menou K., 2009, *ApJ*, 700, 1952
- Haiman Z., Kocsis B., Menou K., Lippai Z., Frei Z., 2009, *Classical and Quantum Gravity*, 26, 094032
- Hayasaki K., 2009, *PASJ*, 61, 65
- Hayasaki K., Mineshige S., Ho L. C., 2008, *ApJ*, 682, 1134
- Hayasaki K., Mineshige S., Sudou H., 2007, *PASJ*, 59, 427
- Hirose S., Krolik J. H., Blaes O., 2009, *ApJ*, 691, 16
- Hobbs et al. 2010, *Classical and Quantum Gravity*, 27, 084013
- Hourigan K., Ward W. R., 1984, *Icarus*, 60, 29
- Ivanov P. B., Papaloizou J. C. B., Polnarev A. G., 1999, *MNRAS*, 307, 79
- Jang-Condell H., Sasselov D. D., 2005, *ApJ*, 619, 1123
- Kley W., Crida A., 2008, *A&A*, 487, L9
- Kocsis B., Frei Z., Haiman Z., Menou K., 2006, *ApJ*, 637, 27
- Kocsis B., Haiman Z., Loeb A., 2012, *MNRAS*, submitted, e-print arXiv:1205.4714 (Paper I)
- Kocsis B., Haiman Z., Menou K., 2008, *ApJ*, 684, 870
- Kocsis B., Sesana A., 2011, *MNRAS*, 411, 1467
- Kocsis B., Yunes N., Loeb A., 2011, *Phys. Rev. D*, 84, 024032
- Kollmeier J. A., Onken C. A., Kochanek C. S., Gould A., Weinberg D. H., Dietrich M., Cool R., Dey A., Eisenstein D. J., Jannuzi B. T., Le Floch E., Stern D., 2006, *ApJ*, 648, 128
- Korycansky D. G., Papaloizou J. C. B., 1996, *ApJS*, 105, 181
- Laughlin G., Steinacker A., Adams F. C., 2004, *ApJ*, 608, 489
- Levin Y., 2007, *MNRAS*, 374, 515
- Lin D. N. C., Papaloizou J., 1986, *ApJ*, 309, 846
- Liu F. K., Wu X.-B., Cao S. L., 2003, *MNRAS*, 340, 411
- Liu Y. T., Shapiro S. L., 2010, *Phys. Rev. D*, 82, 123011
- Lodato G., Nayakshin S., King A. R., Pringle J. E., 2009, *MNRAS*, 398, 1392
- Lubow S. H., D'Angelo G., 2006, *ApJ*, 641, 526
- Lubow S. H., Seibert M., Artymowicz P., 1999, *ApJ*, 526, 1001
- Lynden-Bell D., Pringle J. E., 1974, *MNRAS*, 168, 603
- MacFadyen A. I., Milosavljević M., 2008, *ApJ*, 672, 83
- Madigan A.-M., Levin Y., 2012, *ApJ*, 754, 42
- Masset F. S., Papaloizou J. C. B., 2003, *ApJ*, 588, 494
- McKee C. F., Ostriker E. C., 2007, *ARA&A*, 45, 565
- McKernan B., Ford K. E. S., Kocsis B., Lyra W., Perets H. B., Winter L. M., 2012, in prep.
- McKernan B., Ford K. E. S., Lyra W., Perets H. B., 2012, *ArXiv e-prints*
- Milosavljević M., Phinney E. S., 2005, *ApJ*, 622, L93
- Miralda-Escudé J., Kollmeier J. A., 2005, *ApJ*, 619, 30
- Nelson R. P., Papaloizou J. C. B., 2004, *MNRAS*, 350, 849
- Noble S. C., Mundim B. C., Nakano H., Krolik J. H., Campanelli M., Zlochower Y., Yunes N., 2012, *ArXiv e-prints*
- Novikov I. D., Thorne K. S., 1973, in Dewitt C., Dewitt B. S., eds, *Black Holes (Les Astres Occlus) Astrophysics of black holes..* pp 343–450
- Paardekooper S.-J., Baruteau C., Crida A., Kley W., 2010, *MNRAS*, 401, 1950
- Paardekooper S.-J., Baruteau C., Kley W., 2011, *MNRAS*, 410, 293
- Paardekooper S.-J., Mellema G., 2006, *A&A*, 459, L17
- Paardekooper S.-J., Mellema G., 2008, *A&A*, 478, 245
- Paardekooper S.-J., Papaloizou J. C. B., 2008, *A&A*, 485, 877
- Papaloizou J. C. B., Pringle J. E., 1985, *MNRAS*, 213, 799
- Penna R. F., McKinney J. C., Narayan R., Tchekhovskoy A., Shafee R., McClintock J. E., 2010, *MNRAS*, 408, 752
- Peters P. C., 1964, *Physical Review*, 136, 1224
- Preto M., Berentzen I., Berczik P., Spurzem R., 2011, *ApJ*, 732, L26
- Pringle J. E., 1991, *MNRAS*, 248, 754
- Rafikov R. R., 2012, *ArXiv e-prints*
- Rafikov R. R., Petrovich C., 2012, *ApJ*, 747, 24
- Roedig C., Dotti M., Sesana A., Cuadra J., Colpi M., 2011, *MNRAS*, 415, 3033
- Roedig C., Sesana A., Dotti M., Cuadra J., Amaro-Seoane P., Haardt F., 2012, *MNRAS*, submitted, e-print arXiv:1202.6063
- Schnittman J. D., 2011, *Classical and Quantum Gravity*, 28, 094021
- Sesana A., 2010, *ApJ*, 719, 851
- Sesana A., Haardt F., Madau P., Volonteri M., 2005, *ApJ*, 623, 23
- Sesana A., Roedig C., Reynolds M. T., Dotti M., 2012, *MNRAS*, 420, 860
- Sesana A., Vecchio A., Colacino C. N., 2008, *MNRAS*, 390, 192

- Sesana A., Vecchio A., Volonteri M., 2009, *MNRAS*, 394, 2255
- Shakura N. I., Sunyaev R. A., 1973, *Astron. Astroph.*, 24, 337
- Shapiro S. L., 2010, *Phys. Rev. D*, 81, 024019
- Shen Y., Loeb A., 2010, *ApJ*, 725, 249
- Shi J.-M., Krolik J. H., Lubow S. H., Hawley J. F., 2012, *ApJ*, 749, 118
- Shu F. H., Adams F. C., Lizano S., 1987, *ARA&A*, 25, 23
- Syer D., Clarke C. J., 1995, *MNRAS*, 277, 758
- Tanaka H., Takeuchi T., Ward W. R., 2002, *ApJ*, 565, 1257
- Tanaka T., 2011, *MNRAS*, 410, 1007
- Tanaka T., Haiman Z., Menou K., 2010, *AJ*, 140, 642
- Tanaka T., Menou K., 2010, *ApJ*, 714, 404
- Tanaka T., Menou K., Haiman Z., 2012, *MNRAS*, 420, 705
- Trump J. R., Impey C. D., Kelly B. C., Elvis M., Merloni A., Bongiorno A., Gabor J., Hao H., McCarthy P. J., Huchra J. P., Brusa M., Cappelluti N., Koekemoer A., Nagao T., Salvato M., Scoville N. Z., 2009, *ApJ*, 700, 49
- Ward W. R., 1986, *Icarus*, 67, 164
- Ward W. R., 1988, *Icarus*, 73, 330
- Ward W. R., 1997, *Icarus*, 126, 261
- Ward W. R., Hourigan K., 1989, *ApJ*, 347, 490
- Winters W. F., Balbus S. A., Hawley J. F., 2003, *ApJ*, 589, 543
- Yunes N., Kocsis B., Loeb A., Haiman Z., 2011, *Physical Review Letters*, 107, 171103
- Zel'dovich Y. B., Raizer Y. P., 1967, *Physics of shock waves and high-temperature hydrodynamic phenomena*
- Zhu Y., Davis S. W., Narayan R., Kulkarni A. K., Penna R. F., McClintock J. E., 2012, *ArXiv e-prints*